Supplementary Material for:

Allelic Complexity of *KMT2A* Partial Tandem Duplications in Acute Myeloid Leukemia and Myelodysplastic Syndromes

Harrison K. Tsai[1], Christopher J. Gibson[2], H. Moses Murdock[2], Phani Davineni[5], Marian H. Harris[1], Eunice S. Wang[3], Lukasz P. Gondek[4], Annette S. Kim[5], Valentina Nardi[6], R. Coleman Lindsley[2]

[1]Department of Pathology, Boston Children's Hospital, Harvard Medical School, Boston, MA, USA

[2]Department of Medical Oncology, Dana-Farber Cancer Institute, Harvard Medical School, Boston, MA, USA;

[3]Department of Medicine, Roswell Park Comprehensive Cancer Center, Buffalo, NY

[4]Sidney Kimmel Comprehensive Cancer Center, Johns Hopkins University, Baltimore, MD

[5]Department of Pathology, Brigham and Women's Hospital, Harvard Medical School, Boston, MA, USA

[6]Department of Pathology, Massachusetts General Hospital, Harvard Medical School, Boston, MA, USA

Corresponding Author:

R. Coleman Lindsley, MD, PhD

Dana-Farber Cancer Institute

450 Brookline Avenue

Boston, MA 02215

E-mail: coleman_lindsley@dfci.harvard.edu

Supplementary Methods

DNA sequencing of *KMT2A* and targeted genes: The NGS panels targeted regions of 95-114 genes (HSS v2-v4), 88 genes (RHP v3), or 117 genes and 215 intergenic/SNP loci (MYP), including *KMT2A* exons 1-36 (HSS) or exons 1-13, 24-26, and 28-30 (RHP, MYP) relative to transcript NM_005933.4. Raw sequencing results were processed by clinical or research informatic pipelines consisting of alignment to the hg19 human genome reference through Novoalign v3.0.7.00 (HSS), bwa mem v0.7.17 (RHP), or bwa v0.5.9 (MYH), deduplication by Picard MarkDuplicates v1.128 (HSS) or v1.130 (MYH), reduction of 8 bp unique molecular indexes via fgbio v0.4.0 (RHP), and SNV/indel detection by an ensemble approach (HSS; MuTect v1.1.7, LoFreq v2.1.2, GATK vnightly-2016-01-24-gaa090b7, laboratory developed hotspot caller), VarDict v1.6.0 (RHP), or VarScan v2.3.3 (MYH), where the clinical assays were validated to detect SNV/indels at allelic frequencies of 10% (HSS) or 3% (RHP). *FLT3*-ITD detection was performed by FLT3_ITD_ext v1.1 (HSS, RHP, MYH) and clinically validated for RHP[1]. Copy number variation was assessed and clinically validated through an internally developed algorithm RobustCNV for one of the assays (RHP) and was not performed in the standard pipelines of the other assays (HSS, MYH)[2,3]. Processed results from the informatic pipelines were reviewed manually by molecular pathologists for clinical reporting (HSS: SNV/indels, RHP: SNV/indels and CNV) or underwent internal evaluation (MYH).

Batch Ratios CNV method (BR-CNV): Of the 3 assays, RHP was the only one with a clinically validated pipeline for CNV evaluation, based on a panel of normals (PON), while HSS and MYH did not have CNV assessment or associated sequenced PONs. We thus applied an alternative approach across all three assays. Relative copy numbers were assessed through a batch-based method BR-CNV applied to sequencing batches of 5-27 (HSS), 31 (RHP), and 88 (MYH) samples and predicated on 2 main underlying assumptions: (1) linearity of sequencing read depths for a given target locus relative to copy number (or more specifically, input DNA) and (2) a diploid state over each target locus in the majority of samples of a sequencing batch. Assumption (1) could be evaluated per locus with removal of poorly performing targets, while assumption (2) could only be checked on a broad chromosomal level through concurrent karyotypes and had to be accepted at face value for each specific target, relying instead on the tendency for hematologic genomes to be relatively stable.

For each sample S of a batch and targeted region R specified in assay design bedfiles, mean coverage depth $D_S(R)$ was generated by the clinical and research informatic pipelines from alignments of raw reads (HSS), UMI-consensus reads (RHP), or deduplicated reads (MYH), where counts were extracted from alignment files by either samtools (HSS, RHP) or by Picard CollectHsMetrics (MYH). Each pair of regions R_j and R_k was then associated with a coverage ratio $X_{jkS} = D_S(R_j) / D_S(R_k)$ and a median-adjusted coverage ratio $Y_{jkS} = X_{jkS} / median_T\{X_{jkT}\}$ relative to samples $\{T\}$ in the batch. The relative copy number based on batch ratios of targeted region R_a in sample S was defined as

$$\text{BR-CNV}_S\ (R_a) = median_k\ \{\ Y_{akS} / median_j\{Y_{jkS}\}\ \}$$

For efficiency, it was also possible to fix the value of k, as long as it corresponded to a robust target region R_k, with minimal impact on relative copy numbers.

Relative copy numbers were log2-transformed and underwent circular binary segmentation (CBS) using the R Bioconductor package DNAcopy[4]. Both chromosome 11 and a smaller region around *KMT2A* were separately processed by CBS to have a higher sensitivity for focal copy number changes, and segmentation results with breakpoints in *KMT2A* were manually reviewed. Segmentations with focal gain within the 5' end of *KMT2A* in the absence of copy number loss of 3' *KMT2A* were considered strong evidence *KMT2A*-PTDs when the gain affected a subset of contiguous exons within 2 to 15, and were considered possible *KMT2A*-PTDs when the gain included exon 1. The *KMT2A*-PTD copy number burden was defined as the difference between the segmentation level of the gained segment minus either (i) the average of the surrounding segmentation levels (in most cases) or (ii) the segmentation level of 3' *KMT2A* in rare instances of definitive distal 11q gain.

BR-CNV was further modified to optionally integrate a panel of normals (PON) when available. RHP had an available PON which consisted of 2 sub-batches PON_0 and PON_1 that were sequenced during the original validation of the RHP assay The overall strategy was to adjust coverage ratios of the normal samples in PON_0 and PON_1 by scaling to match medians of any given clinical batch, and then to use unadjusted normals, adjusted normals, and the clinical batch median to determine a "nearest normal" to a clinical sample and finally calculate copy numbers relative to this nearest normal. Specifically, coverage ratios of normal samples in PON_0 and PON_1 were scaled respectively by the multiples $c_{jk} = (median_T\{X_{jkT}\}/median_N\{X_{jkN}\})$ and $c'_{jk} = (median_T\{X_{jkT}\}/median_{N'}\{X_{jkN'}\})$ where $\{N\}$, $\{N'\}$, and $\{T\}$ denote all samples of PON_0, PON_1, and the clinical batch. Given a clinical sample S, the "nearest normal" (NN) was then defined in terms of the coefficients $\{p^*_N, p^*_{N'}, q^*_N, q^*_{N'}, r^*\}$ solving the linear program:

$$\text{Minimize } \sum_{j,k}(X_{jkS} - (\sum_{N} p_N X_{jkN} + \sum_{N'} p_{N'} X_{jkN'} + \sum_{N} q_N c_{jk} X_{jkN} + \sum_{N'} q_{N'} c'_{jk} X_{jkN'} + r\,[median_T\{X_{jkT}\}]))^2$$

$$\text{where } \sum_{N} p_N + \sum_{N'} p_{N'} + \sum_{N} q_N + \sum_{N'} q_{N'} + r = 1 \text{ and all } p_N \geq 0,\ p_{N'} \geq 0,\ q_N \geq 0,\ q_{N'} \geq 0,\ r \geq 0.$$

The PON-based relative copy number is finally:

$$\text{PON-BR-CNV}_S\ (R_a) = median_k\ \{ X_{akS} / NN_{akS} \}$$

$$NN_{akS} = \sum_{N} p^*_N X_{akN} + \sum_{N'} p^*_{N'} X_{akN'} + \sum_{N} q^*_N c_{ak} X_{akN} + \sum_{N'} q^*_{N'} c'_{ja} X_{akN'} + r^*\,[median_T\{X_{akT}\}]$$

We also remark that our methods relied on batch sequencing of general hematologic samples and may be subject to error in heavily biased cohorts that shift the median, in contrast to the use of a matched sample in the Sun study[5]. Our methods were also independent of isoform, whereas the metric in the Sun study was optimized to exons 2-8 potentially biasing assessment of *KMT2A*-PTDs spanning different exons.

SNP analysis of NGS data and KASUMI6: SNP profiles were constructed over chromosome 11 for each of the cohorts and their respective assays (HSS, RHP, MYH) as follows. A master bedfile of effective coverage consisting of any genomic location of chromosome 11 with coverage $\geq$ 100 (HSS) or 50 (RHP, MYH) in at least one sample was first generated through "samtools depth". The intervals of this bedfile were then cross-referenced with gnomAD v2.1.1 exomes and genomes obtained through Google colab and its BigQuery interface into gnomAD. A master SNP bedfile was next constructed consisting of genomic positions having population allelic frequency $\geq$ 0.0001 for an ALT SNP (not indels), and these positions were subsequently evaluated for each sample through "samtools mpileup" to produce SNP profiles. A subset of these SNP genomic locations were subject to recurrent artifacts (e.g. from repetitive sequence, multi-mapping, etc), making estimation of allelic fractions unreliable. Suboptimal locations with a high empirical proportion of allelic fractions away from 0, 0.5, or 1 were identified and excluded. Other locations were subject to systematic bias for estimating the heterozygous state due to likely differential binding of probes or primers, and this was recognized through histograms and violin plots of empiric allelic fraction distributions. CN-LOH was assessed by manual review of the resulting SNP profiles, in conjunction with copy number profiles by BR-CNV, available karyotypic information, and empiric background distributions. SNP analysis of the KASUMI6 cell line was performed by downloading publicly available raw Cytoscan HD SNP array data (GSM4254134_Kasumi-6_CytoScanHD_Array_.CEL.gz) from Gene Expression Omnibus and re-processing it with the package Rawcopy (https://hub.docker.com/r/rawcopy/rawcopy; downloaded 08/30/2020) to obtain B-allele frequencies over chromosome 11[6,7]. Cystoscan HD array SNP sites within candidate regions of CN-LOH in KASUMI6 were then queried in genotypes from the 1000 Genomes project (ALL.chr11.shapeit2_integrated_snvindels_v2a_27022019.GRCh38.phased.vcf.gz; downloaded 09/24/2020 from www.internationalgenome.org/data-portal) to determine a population distribution of heterozygous SNP counts over those sites.

Estimates of *KMT2A*-PTD allelic fractions from copy number levels: The allelic fraction (AF) of a *KMT2A*-PTD was defined as the ratio

AF = (copy number of *KMT2A*-PTD exons) / (copy number of distal *KMT2A* exons) - 1

In most circumstances, this ratio represented the bulk average of the number of *KMT2A*-PTD copies in a cell divided by the total number of wild-type and *KMT2A*-PTD copies, similar to the definition of an allelic fraction of a single nucleotide variant. For example, the AF of a cell with a *KMT2A*-PTD allele and a wild-type allele was 0.5 while a cell with a *KMT2A*-PTD allele that underwent CN-LOH was 1. In theory, this definition of AF could also exceed 1 due to copy number contributions that were not technically *KMT2A*-PTDs, for example episomal amplification or higher order linear replications (triplications, etc) producing the same breakpoint as a *KMT2A*-PTD, however the existence of these variants has not been reported before to our knowledge. Other structural variants involving *KMT2A* could also affect the AF, such as non-balanced rearrangements or those associated with gain, however these would generally not cause the AF to exceed 1 and would have different breakpoints from a *KMT2A*-PTD.

Split-read based detection, characterization, and allelic-fraction estimates of structural variants: Raw reads aligning to *KMT2A* were extracted from bamfiles generated by the standard pipelines prior to deduplication or UMI reduction, and realigned with bwa-mem v0.7.17 to hg19 for the case of HSS and MYH whereas RHP already used bwa-mem as its de facto aligner. Read pairs satisfying relatively stringent alignment criteria (concordant under bwa-mem with insertions totaling ≤2 bp, deletions totaling ≤2 bp, soft clips totaling ≤2 bp, and edit distance ≤5 bp in each read of a pair) were categorized as reference-reads and set aside for use in allelic-fraction estimates. Split-reads were defined as single ends of non-reference-reads having one (or rarely two) supplementary alignments under bwa-mem, and were each associated with a breakpoint signature consisting of a supplementary breakpoint, primary breakpoint, and overlap for every supplementary alignment, where the overlap could be positive (shared microhomology), negative (intervening unaligned sequence), or zero. Every breakpoint signature was further associated with a pair (or rarely triplet) of core CIGAR strings stripped of soft-clip and hard-clip components from the primary and secondary alignments. To minimize artifactual false positives, breakpoint signatures needed to either be (i) common to 3 or more split-reads with at least 3 different core CIGAR pairs or (ii) previously identified in the setting of a serial sample to undergo further consideration. Associated split-reads were next extended in-silico along reference chromosomes away from breakpoints to reach the nearest whole 1 kbp genomic coordinate at least 500 bp away from a breakpoint. Extended reads were then clustered into representatives referred to as structural variant mini-genomes, and the locations of mutant breakpoints along mini-genomes were determined from breakpoint signatures. Supporting mutant reads were identified by aligning non-reference reads directly to a mini-genome via bwa-mem and keeping paired-reads satisfying relatively stringent alignment criteria (concordant alignments extending 10 bp or more past a mutant breakpoint location in at least one read of the pair, and otherwise having insertions totaling ≤2 bp, deletions totaling ≤2 bp, soft clips totaling ≤2 bp, and edit distance ≤5 bp in each read of the pair). Mutant read counts, depth of coverage by genomic position, and breadth of coverage by genomic position, especially over the region bounded by mutant breakpoint(s) in the mini-genome, were used to evaluate the strength of evidence for a structural variant.

To estimate allelic fractions, supporting mutant reads were compared to reference reads that also extended 10 bp or more past a mutant breakpoint in at least one read of a pair, and additionally satisfied platform-specific criteria. For HC (MYH), applicable reference reads were further limited to sequenced fragments whose inferred centers were located proximal to the mutant breakpoint in order to exclude fragments that were more likely captured by baits past a mutant junction and thus not capable of hybridizing to a mutant genome. For AMP (HSS) and NEB (RHP), applicable reference reads were further limited to fragments derived from GSP2s (AMP) or baits (RHP) proximal to the mutant junction, which could be determined in these assays by alignment of the 5' end of R2 (read 2). For general rearrangements, the allelic fraction was then calculated as [mutant reads / (mutant reads + reference reads)] similar to SNVs. For *KMT2A*-PTDs, the allelic fraction was calculated as [mutant reads / reference reads] since PTD alleles were capable of generating mutant and reference reads. In particular, although PTD alleles initially appeared twice as likely in theory to generate fragments overlapping reference boundaries versus mutant junctions of a duplication, the platform specific criteria enabled proper accounting of supporting mutant reads and applicable reference reads.

<u>RNA-sequencing analysis of *KMT2A*-PTDs in CCLE and clinical data</u>: Select clinical samples from the MGH cohort were concurrently tested by a targeted RNA-based NGS panel (Heme Fusion Assay: HFA) also derived from anchored multiplex PCR (AMP; ArcherDx, Boulder, CO) that was clinically validated to report pathogenic KMT2A-PTD isoforms (RNA/DNA cohort: n=350). Clinical RNA data (HFA) of *KMT2A*-PTDs in the MGH RNA/DNA cohort was assessed by identifying and counting split-read alignments in the HFA bamfiles (generated by bwa-mem) that corresponded to mutant or wild-type junctions and that originated from anchored primers capable of sequencing across the *KMT2A*-PTD mutant junction. Compressed fasta files were downloaded from SRA by fastq-dump for select CCLE cell-lines: EOL1 (SRR8616218), KASUMI6 (SRR8615363), HL60 (SRR8616133), OCI-AML3 (SRR8615242), and KASUMI1 (SRR8615361). Paired-end reads containing certain exon:exon junctions of 30 bp length were identified and counted in the fasta files by "zgrep -B1" applied to the following sequences: (1) exon8:exon2 mutant junction (AAACCAAAAGAAAAGGATGAGCAATTCTTA and its reverse complement TAAGAATTGCTCATCCTTTTCTTTTGGTTT), (2) exon8:exon9 wild-type junction (AAACCAAAAGAAAAGGAAAAACCACCTCCG and its reverse complement CGGAGGTGGTTTTTCCTTTTCTTTTGGTTT), and (3) exon1:exon2 wild-type junction (GGCGGCAGCGGAGAGGATGAGCAATTCTTA and its reverse complement TAAGAATTGCTCATCCTCTCCGCTGCCGCC).

Supplemental Tables.

Table S1. Relative enrichment of co-occurring gene mutations in AML subgroups based on inferred *KMT2A*-PTD allelic status. Complex or high copy ratio PTD (n=38) versus remaining low copy ratio PTD (n=35). Genes that were recurrently mutated (2 or more times) in at least one of the subgroups are listed in the table. p-values are from Fisher's exact test.

Gene	Complex or <u>High Ratio</u> # of 38 (%)	Remaining <u>Low Ratio</u> # of 35 (%)	<u>p-value</u> (Fisher)
FLT3-ITD	15 (39.5%)	6 (17.1%)	0.042
DNMT3A	15 (39.5%)	9 (25.7%)	0.226
IDH2	13 (34.2%)	9 (25.7%)	0.456
RUNX1	10 (26.3%)	14 (40.0%)	0.319
U2AF1	7 (18.4%)	10 (28.6%)	0.408
STAG2	6 (15.8%)	8 (22.9%)	0.556
WT1	5 (13.2%)	0 (0%)	0.055
NF1	5 (13.2%)	1 (2.9%)	0.201
TET2	5 (13.2%)	7 (20%)	0.533
ASXL1	5 (13.2%)	9 (25.7%)	0.237
PTPN11	4 (10.5%)	1 (2.9%)	0.359
IDH1	4 (10.5%)	4 (11.4%)	1
NRAS	3 (7.9%)	4 (11.4%)	0.703
CALR	2 (5.3%)	0 (0%)	0.494
ZRSR2	2 (5.3%)	0 (0%)	0.494
SMC1A	2 (5.3%)	0 (0%)	0.494
ATM	2 (5.3%)	1 (2.9%)	1
CBL	2 (5.3%)	2 (5.7%)	1
PHF6	2 (5.3%)	2 (5.7%)	1
JAK2	2 (5.3%)	3 (8.6%)	0.666
BCOR	2 (5.3%)	4 (11.4%)	0.418
TP53	2 (5.3%)	5 (14.3%)	0.249
SRSF2	2 (5.3%)	8 (22.9%)	0.041
FLT3-TKD	1 (2.6%)	2 (5.7%)	0.604
CEBPA	1 (2.6%)	3 (8.6%)	0.344
DDX41	0 (0%)	2 (5.7%)	0.226
GATA2	0 (0%)	2 (5.7%)	0.226
EZH2	0 (0%)	2 (5.7%)	0.226

Supplementary Figure Legends

Figure S1. Validation of BR-CNV estimates across general loci. Copy number estimates by BR-CNV of chromosome 21 in cases of AML of Down syndrome and various other genomic loci compared to clinical FISH data. Total copy number levels were obtained by integrating karyotype data to identify the diploid baseline.

Figure S2. BR-CNV estimates of *KMT2A*-PTD exons. (A) Comparisons on 7 cases sequenced by both RHP and HSS with known *KMT2A*-PTDs identified by clinical RNA testing (HFA). Average levels of chromosome 15 targets were also compared, where 3 cases had trisomy 15 by karyotype. (B) Estimates by BR-CNV versus RobustCNV for RHP data, where RHP was the only assay with clinically validated copy number calling.

Figure S3. Split-reads enable estimates of structural variant and *KMT2A*-PTD VAFs. (A) Split-read based estimates of *KMT2A* rearrangements compared to concurrent clinical *KMT2A* FISH. Since traditional validation of split-read based accuracy for *KMT2A*-PTD quantification was not possible due to lack of an orthogonal quantitative clinical assay, a limited proof of principle was instead established through (non-PTD) *KMT2A* rearrangements quantified by clinical FISH testing. As a side benefit from this effort, *KMT2A* split-reads revealed breakpoints of several novel (non-PTD) *KMT2A* rearrangements of unknown significance (*KMT2A-AHCYL2*, *LINC01531-KMT2A, MECR-KMT2A*, and *KMT2A-GATAD2*), and demonstrated a sensitivity of 55% (6/11) and specificity of 100% (5/5) relative to cytogenetics in one of the assays (RHP) despite not explicitly targeting *KMT2A* introns. (B) Split-read versus BR-CNV estimates of *KMT2A*-PTD copy number ratios, restricted to cases detected by both BR-CNV and split-read analysis with coverage depth above 200 around the breakpoints (split-reads + reference reads). Since BR-CNV estimates correlated with FISH over various loci (Figure S1), BR-CNV was extrapolated to perform well across the targeted genome including *KMT2A*.

Figure S4. Split-reads help resolve potentially ambiguous copy number signals and unusual *KMT2A*-PTD cases. (A-B) A common challenge occurred when partial *KMT2A* copy number gain included exon 1, which represented multiple possibilities: (i) a non-standard *KMT2A*-PTD spanning exons 1-8 (panel A) where split-reads confirmed genomic breakpoints in intron 8 and immediately proximal to exon 1, (ii) *KMT2A* rearrangement, especially *KMT2A-MLLT10*, where partial duplication of the 5' segment of *KMT2A* is known to occur rarely but recurrently[8-10] and was seen in a case from our elderly AML cohort (panel B) with gain of *KMT2A* exons 1-6 by BR-CNV and evidence of *KMT2A-MLLT10* by both karyotype and explicit split-read capture of genomic breakpoints, and (iii) mischaracterization of the copy number level of exon 1 due to copy number noise exacerbated by high GC content, which occurred in a few cases demonstrating discordant *KMT2A*-PTD boundaries from DNA versus RNA testing. (C) Integration of split-reads and copy number data showed promise at characterizing rare difficult cases, including an elderly AML case where split-reads involving *KMT2A* intron 8 and chromosome 4 were insufficient to explain the magnitude of copy number gain of *KMT2A* exons 2-8; moreover, *KMT2A* exon 1 demonstrated gain to a lesser magnitude than exons 2-8, raising the possibility of a separate *KMT2A*-PTD. Not shown: Although extremely rare, copy number gains not including exon 1 also may potentially represent false positives; namely, *KMT2A-AF9* expression has been reported as the predominant transcript from non-tandem duplication of *KMT2A* exons 2-8 interrupted by insertion of 3' *AF9*, albeit in a B-ALL case and not a myeloid malignancy[11].

Figure S5. Collection of *KMT2A*-PTD genomic breakpoints detected by split-reads. Breakpoints in close proximity to or occasionally within targeted *KMT2A* exons were sequenced by our NGS assays and identified as chimeric split-read alignments in 28% (26/94) of patients

with *KMT2A*-PTDs, corresponding to 25 unique breakpoint pairs. Novel isoforms e13e3 (2 patients), e15e2 (1 patient), and e6e2 (1 patient) were predicted from breakpoints in i13e2 and i13i2, i15i1, and i6i1 respectively. The isoform e6e2 would be out-of-frame (thus atypical), raising the question of whether e6e3 transcripts might be generated by alternative splicing. The isoform e15e2 was unusual for its subclonal status (described further in Figure S7) and thus considered to have uncertain clinical significance. The breakpoint i8pre was predicted to generate the e8e2 isoform given the lack of a 3' splice acceptor site before exon 1. +XXX: intervening exogenous filler sequence. mh: microhomology. e: exon. i: intron. pre: 5' of *KMT2A*.

Figure S6. *KMT2A*-PTDs assessed by split-reads below the limit of detection of BR-CNV. (A) A novel *KMT2A*-PTD involving exons 2-15 was present at multiple timepoints as a minor subclone relative to moderate blast percentages and presumptive clonal mutations in *TP53* and *DDX41*, with split-read based VAFs of 1.0% (15 split-reads / 1484 reference), 3.0% (69/2327), and 2.1% (53/2481). While not detected by BR-CNV, the high coverage over the genomic breakpoints enabled a relatively low limit of detection by split-reads. The biological significance was less certain given the low subclonal VAF, contrary to typical pathogenic *KMT2A*-PTDs arising in predominant clones as early cooperating mutations critical to AML development[5]. Clinical RNA testing also revealed aberrant expression of the e15e2 isoform. To our knowledge, little is known about *KMT2A*-PTDs in *DDX41*-related AML. (B) Split-reads from an intronic area with low coverage yielded inaccurate estimates for a *KMT2A*-PTD involving exons 2-10 from a second *DDX41*-related AML but were still present at a timepoint with low-level measurable residual disease (MRD). In general, chimeric *KMT2A*-PTD split-reads from the pathogenic isoforms did not arise as recurrent DNA artifacts (sequencing, chemical, or PCR), thus may enable low limit of quantification in conjunction with optimizing targeted regions, sequencing depths, and DNA input for purposes of MRD assessment.

Figure S7. Incidence of *KMT2A*-PTD in sequential clinical cohorts of hematologic disease. *KMT2A*-PTD was identified only in AML and MDS cases among all samples tested at 2 institutions (BWH, MGH; n=8770), consistent with prior studies[5]. In a well-annotated cohort of new diagnoses (BWH 2019-2020; n=476), *KMT2A*-PTDs were present in 6.1% (10/165) of AML and 10.0% (5/49) of MDS diagnoses but not in other myeloid diseases (Ph-negative myeloproliferative neoplasms, CML, CNL), lymphoid diseases (non-Hodgkin lymphoma, B-ALL, T-ALL, MM, HCL, LGL) or non-clonal hematologic diseases (AA, HLH). AA: aplastic anemia, AML: acute myeloid leukemia, B-ALL: B-cell acute lymphoblastic leukemia, BPCDN: blastic plasmacytoid dendritic cell neoplasm, CNL: chronic neutrophilic leukemia, CML: chronic myeloid leukemia, ET: essential thrombocytopenia, HCL: hairy cell leukemia, HLH: hemophagocytic lymphohistiocytosis, LGL: large granular lymphocytic leukemia, LYMPH: lymphoma, MAST: mastocytosis, MDS: myelodysplastic syndrome, MM: multiple myeloma, MPN: myeloproliferative neoplasm (other), PMF: primary myelofibrosis, PV: polycythemia vera, T-ALL: T-cell acute lymphoblastic leukemia.

Figure S8. *KMT2A*-PTDs with gain of 11q23.3 from the *KMT2A*-PTD allele. (A-C) Copy number profiles of P1-P3 were shown in Figures 1A-B and partially in Figure 2A. They are included here for completeness. (D) Serial copy number profiles of P4 (AML), which initially harbored a simple PTD and relapsed after transplant with appearance of 11q23.3 gain from the PTD allele and subsequent outgrowth of this clone prior to death. (E) Gain of 11q23.3 analysis for P1-P4. Serial samples from P3 and P4 were shown in Figures 2C-D, and are included here for completeness. P1 corresponded to ~92% complex PTD (with 11q23 gain from the PTD allele), ~3% simple PTD, and ~5% wild-type (non-PTD). P2 existed on the lower line of the larger triangle (connecting vertices of 100% wild-type and 100% complex with double PTD gain)

and corresponded to ~70% complex PTD (with double gain of 11q23 from the PTD allele) and ~30% wild type (non-PTD cells), with negligible simple PTD component (see also Figure 1B).

Figure S9. CN-LOH of *KMT2A*-PTDs from the elderly AML cohort. (A-D) Four cases (P5-P8) demonstrated *KMT2A*-PTDs with CN-LOH, where P5 and P8 were described in Figure 1E-F and are included here for completeness. P5 and P7 were associated with normal karyotypes, whereas *KMT2A*-PTD in AML with normal cytogenetics has previously been thought to affect only a single allele[12]. CN-LOH generally spanned the targeted and occasional off-target regions of 11q, where additional involvement of the 11p arm could not always be excluded. P8 demonstrated 5.55 copies of *KMT2A* exons 2-8 with no other identified copy number changes. Moreover, the gain was entirely attributable to a single PTD mutant junction connecting intron 8 to intron 1 since split-reads yielded a copy number estimate of 5.28 similar to the BR-CNV estimate of 5.55. This magnitude of gain in the context of a single mutant junction raised the possibility of a different mechanism such as intrachromosomal or episomal amplification. P7 similarly demonstrated 4.88 copies of *KMT2A* exons 2-8 suggestive of intrachromosomal or episomal amplification. The MYH assay targeted 4 common SNP regions and the genes *EED*, *ATM*, *KMT2A*, and *CBL* along 11q while additionally benefitting from off-target coverage of a few extra 11q regions. The design yielded an empirical median coverage of 26 heterozygous 11q SNPs per case (range 6-54) and enabled relatively robust detection of broad 11q CN-LOH. Across the entire elderly AML cohort, CN-LOH of 11q was thereby also detected in 5 separate AMLs harboring *CBL* mutations but not *KMT2A*-PTD, and 2 AMLs with no identifiable 11q variants among the targeted genes. Since LOD of NGS assays is dictated by the number of heterozygous SNPs in a region of CN-LOH relative to VAF noise, we expected LOD to be roughly 30% for broad 11q CN-LOH, similar to WES for CN-LOH of 10 Mb regions[13], although we did not formally investigate this using serial dilutions and gold standards. In P5 (A), CN-LOH was estimated to involve approximately 40% of cells based on VAFs of heterozygous SNPs, where the signal for allelic imbalance was robustly distinguishable from noise and predicted to persist down to 30% involvement of cells by simple modeling.

Figure S10. CN-LOH of *KMT2A*-PTDs from the clinical BWH and MGH cohorts. (A-G) Seven cases (P9-P15) tested by the clinical NGS assays demonstrated *KMT2A*-PTDs with CN-LOH and were associated with normal (2), simple (4), and unknown karyotypes (1). The cases were comprised of 4 MDS (P9-P11, P15) and one PV (P12) with secondary AML transformation, one MDS (P13) without progression, and one myeloid sarcoma (P14). Due to limited targeted coverage of 11q in the clinical assays, a few of these cases had informative SNPs adjacent to *KMT2A* but not spanning both sides; nevertheless, involvement of the *KMT2A* locus was inferred as the explanation of high copy number gain. SNP analysis was occasionally complicated by transplant status but could be resolved in the context of low donor chimerism (P11).

Figure S11. Focal CN-LOH can affect *KMT2A*-PTD. (A) The KASUMI6 cell line demonstrated 0 heterozygous SNPs over 177 consecutive sites of the CytoscanHD array between chr11:117,619,027-118,938,315 (~1.3 Mb) containing *KMT2A* but not *CBL*. (B) By contrast, 2584 HapMap genomes had a median of 36 heterozygous SNPs and never 0 (range 6-92) over these 177 sites. Combined with the high copy number gain of exons 2-8 beyond the level of a monoallelic *KMT2A*-PTD[5], the findings support interstitial focal CN-LOH. KASUMI6, derived from relapsed AML, may thus provide a model of biallelic *KMT2A*-PTD, whereas many studies[14,15] have used EOL1, derived from a *FIP1L1-PDGFRA*-associated chronic eosinophilic leukemia harboring a simple *KMT2A*-PTD. RNA expression of the e8e2 mutant junction in KASUMI6 was accordingly increased compared to EOL1 (Figure S12).

Figure S12. *KMT2A*-PTD RNA expression is correlated with DNA allelic burden. Our cohorts contained 30 *KMT2A*-PTD samples from 20 patients with concurrent DNA-based (HSS) and RNA-based (HFA) targeted NGS panel testing, while the cell lines KASUMI6 and EOL1 had CCLE public data from whole-transcriptome RNA-seq and Affymetrix Genome-Wide Human SNP Array 6.0. RNA reads containing the mutant splice junction were normalized relative to reads containing reference splice junctions, which could be derived from mutant or wild-type transcripts since tandem duplications contained both mutant and wild-type junctions. In KASUMI6, this analysis confirmed the presence of aberrant RNA reads spanning the *KMT2A* exon8:exon2 mutant splice junction. These mutant reads were uncharacterized and not aligned to the *KMT2A* locus in the processed CCLE bam file but were present in the raw FASTQ files at a similar level to reads spanning exon8:exon9 or exon1:exon2 wild-type junctions and moreover persisted after polyA enrichment in the RNA-seq protocol, thus consistent with transcripts from genomic duplication (*KMT2A*-PTD) versus the alternative possibility of backspliced circular RNAs. CCLE: Cancer Cell Line Encyclopedia. AMP: anchored multiplex PCR used by the HFA and HSS assays. WT: wild-type. SR: split-read. VAF: variant allele fraction.

Figure S13. Evolution of *KMT2A*-PTD and co-mutations across serial samples. (A) In P3, *KMT2A*-PTD complexity (described in Figure 2B-C) was the only identifiable clonal event tracking the evolution of blasts at the final time point of progression. Distal gain complexity was not detectable by bulk NGS at the intermediate time point of first AML diagnosis (d112), however its subclonal presence at AML diagnosis could be deduced from clonal hierarchy. Namely, an *NRAS* hotspot variant was inferred as subclonal to the complex *KMT2A*-PTD based on initial absence at the MDS time point and the estimated clone sizes at the final time point implying cells harboring both complexity and the *NRAS* mutation (70% cells with complex *KMT2A*-PTD, 30% cells with simple *KMT2A*-PTD, and 35% cells with *NRAS* corresponding to 17.5% VAF) (see also Figure 2C). Thus, the emergence of the *NRAS* variant at AML diagnosis (1.4% VAF; 2.8% cells) implied the presence of *KMT2A*-PTD complexity below the limit of NGS detection but in at least 2.8% cells. (B) In P4 (described in 2C), an initially subclonal *NF1* loss-of-functon SNV grew out as the dominant clone at relapse. The initial timepoint also had single copy loss of *NF1* at a relatively high inferred allelic fraction, thus the *NF1* SNV was likely already associated with LOH at the initial timepoint. Detectable *KMT2A*-PTD complexity emerged at relapse. Estimated percent tumor cells involved by *KMT2A*-PTD complexity after relapse (48%, 73%, and 96%) suggested a subclonal relationship to the biallelic *NF1* alterations (61%, 76%, and 88%) with relative outgrowth of the subclone. (C) In P6, a *RUNX1* variant with CN-LOH was newly detected and the dominant clone upon MDS relapse and expanded during AML progression. A simple *KMT2A*-PTD was present at the initial MDS time point prior to relapse, and experienced CN-LOH during tumor evolution, however a robust CN-LOH signal from imbalanced heterozygous SNPs was only possible at the final time point (AML) due to earlier chimeric states from transplant. Estimated percentage of involved tumor cells was again less for the complex *KMT2A*-PTD event (88%) compared to *RUNX1* (96%) at the final time point, suggesting an evolutionary timeline in the predominant clone of a parental simple *KMT2A*-PTD followed by *RUNX1* SNV and CN-LOH events, followed by *KMT2A*-PTD CN-LOH.

Figure S14. Co-occurring gene mutations relative to inferred *KMT2A*-PTD allelic status in AML. Comparison of AML with complex or high ratio *KMT2A*-PTD (n=38) versus remaining AML with low-ratio *KMT2A*-PTD (n=35). See Table S1 for statistical significance.

Figure S15. Proportions of allelic patterns and inferred complexity of *KMT2A*-PTD. (A) Selective 11q23 gain of the PTD allele was observed in 4/94 (4%) of *KMT2A*-PTD patients while broad 11q CN-LOH of the PTD allele was observed in 11/94 (12%) of *KMT2A*-PTD patients. (B)

Indirect evidence of PTD allelic complexity based on high copy ratios above 1.6 at any time point was observed in 42/94 (45%) of *KMT2A*-PTD patients.

Supplementary References

1. Tsai HK, Brackett DG, Szeto D, Frazier R, MacLeay A, Davineni P, et al. Targeted Informatics for Optimal Detection, Characterization, and Quantification of FLT3 Internal Tandem Duplications Across Multiple Next-Generation Sequencing Platforms. J Mol Diagn 2020;22(9):1162-1178.
2. Bi WL, Greenwald NF, Ramkissoon SH, Abedalthagafi M, Coy SM, Ligon KL, et al. Clinical Identification of Oncogenic Drivers and Copy-Number Alterations in Pituitary Tumors. Endocrinology 2017;158(7):2284-2291.
3. Hinohara K, Wu HJ, Vigneau S, McDonald TO, Igarashi KJ, Yamamoto KN, et al. KDM5 Histone Demethylase Activity Links Cellular Transcriptomic Heterogeneity to Therapeutic Resistance. Cancer Cell 2018;34(6):939-953.
4. Olshen AB, Venkatraman ES, Lucito R, Wigler M. Circular binary segmentation for the analysis of array-based DNA copy number data. Biostatistics. 2004 Oct;5(4):557-72.
5. Sun QY, Ding LW, Tan KT, Chien W, Mayakonda A, Lin DC, et al. Ordering of mutations in acute myeloid leukemia with partial tandem duplication of MLL (MLL-PTD). Leukemia 2017;31(1):1-10.
6. Kasai F, Asou H, Ozawa M, Kobayashi K, Kuramitsu H, Satoh M, et al. Kasumi leukemia cell lines: characterization of tumor genomes with ethnic origin and scales of genomic alterations. Hum Cell 2020;33(3):868-876.
7. Mayrhofer M, Viklund B, Isaksson A. Rawcopy: Improved copy number analysis with Affymetrix arrays. Sci Rep 2016;6:36158. doi: 10.1038/srep36158.
8. Jarosova M, Takacova S, Holzerova M, Priwitzerova M, Divoka M, Lakoma I, et al. Cryptic MLL-AF10 fusion caused by insertion of duplicated 5' part of MLL into 10p12 in acute leukemia: a case report. Cancer Genet Cytogenet 2005;162(2):179-82.
9. Sárová I, Brezinová J, Zemanová Z, Izáková S, Lizcová L, Malinová E, et al. Cytogenetic manifestation of chromosome 11 duplication/amplification in acute myeloid leukemia. Cancer Genet Cytogenet 2010;199(2):121-7.
10. Fukushima H, Nanmoku T, Hosaka S, Yamaki Y, Kiyokawa N, Fukushima T, et al. The Partial Duplication of the 5' Segment of KMT2A Revealed KMT2A-MLLT10 Rearrangement in a Boy with Acute Myeloid Leukemia. Case Rep Pediatr 2017;2017:6257494.
11. Whitman SP, Strout MP, Marcucci G, Freud AG, Culley LL, Zeleznik-Le NJ, et al. The partial nontandem duplication of the MLL (ALL1) gene is a novel rearrangement that generates three distinct fusion transcripts in B-cell acute lymphoblastic leukemia. Cancer Res 2001;61(1):59-63.
12. Caligiuri MA, Strout MP, Oberkircher AR, Yu F, de la Chapelle A, Bloomfield CD. The partial tandem duplication of ALL1 in acute myeloid leukemia with normal cytogenetics or trisomy 11 is restricted to one chromosome. Proc Natl Acad Sci USA 1997;94(8):3899-902.
13. San Lucas FA, Sivakumar S, Vattathil S, Fowler J, Vilar E, Scheet P. Rapid and powerful detection of subtle allelic imbalance from exome sequencing data with hapLOHseq. *Bioinformatics*. 2016;32(19):3015-7.
14. Kuhn MW, Hadler MJ, Daigle SR, Koche RP, Krivtsov AV, Olhava EJ, et al. MLL partial tandem duplication leukemia cells are sensitive to small molecule DOT1L inhibition. Haematologica 2015;100(5):e190-3.
15. Bera R, Chiu MC, Huang YJ, Huang G, Lee YS, Shih LY. DNMT3A mutants provide proliferating advantage with augmentation of self-renewal activity in the pathogenesis of AML in KMT2A-PTD-positive leukemic cells. Oncogenesis 2020;9(2):7.

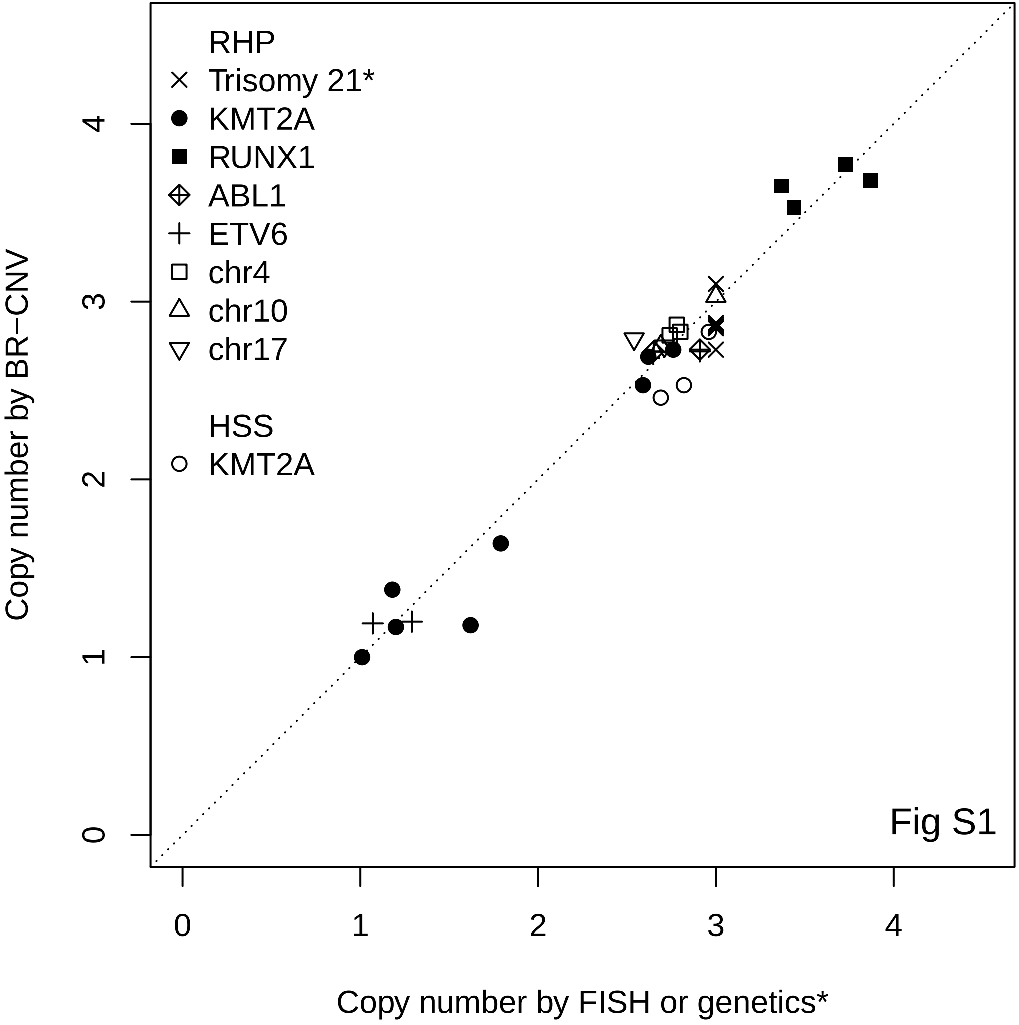

Fig S1

RHP
× Trisomy 21*
● KMT2A
■ RUNX1
⊕ ABL1
+ ETV6
□ chr4
△ chr10
▽ chr17
HSS
○ KMT2A
Copy number by BR−CNV
0
1
2
3
4
Copy number by FISH or genetics*
0
1
2
3
4

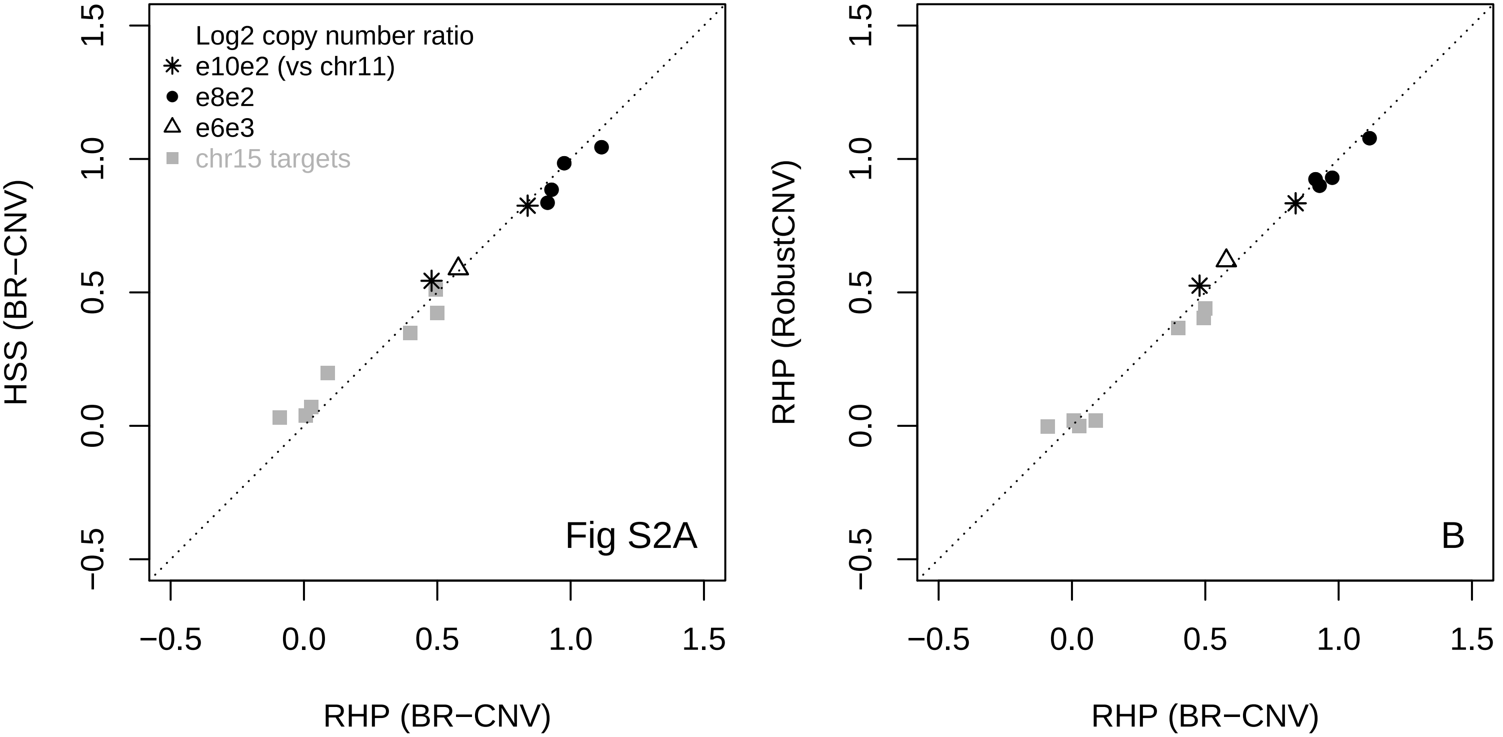
Log2 copy number ratio
✳ e10e2 (vs chr11)
● e8e2
△ e6e3
■ chr15 targets
Fig S2A
HSS (BR−CNV)
RHP (BR−CNV)
−0.5
0.0
0.5
1.0
1.5
B
RHP (RobustCNV)
RHP (BR−CNV)

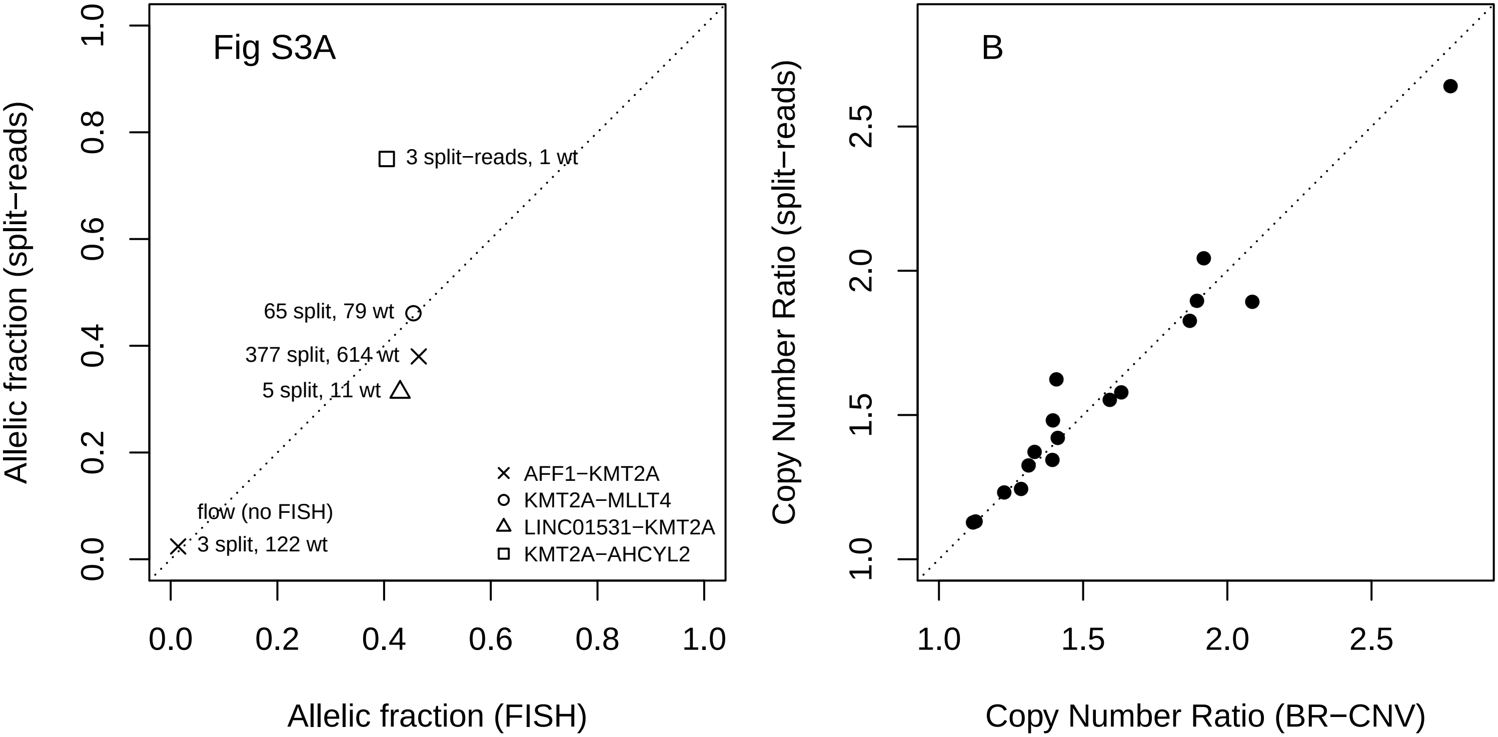
Fig S3A
3 split−reads, 1 wt
65 split, 79 wt
377 split, 614 wt
5 split, 11 wt
flow (no FISH)
3 split, 122 wt
× AFF1−KMT2A
○ KMT2A−MLLT4
△ LINC01531−KMT2A
□ KMT2A−AHCYL2
Allelic fraction (split−reads)
0.0
0.2
0.4
0.6
0.8
1.0
Allelic fraction (FISH)
0.0
0.2
0.4
0.6
0.8
1.0
B
Copy Number Ratio (split−reads)
1.0
1.5
2.0
2.5
Copy Number Ratio (BR−CNV)
1.0
1.5
2.0
2.5

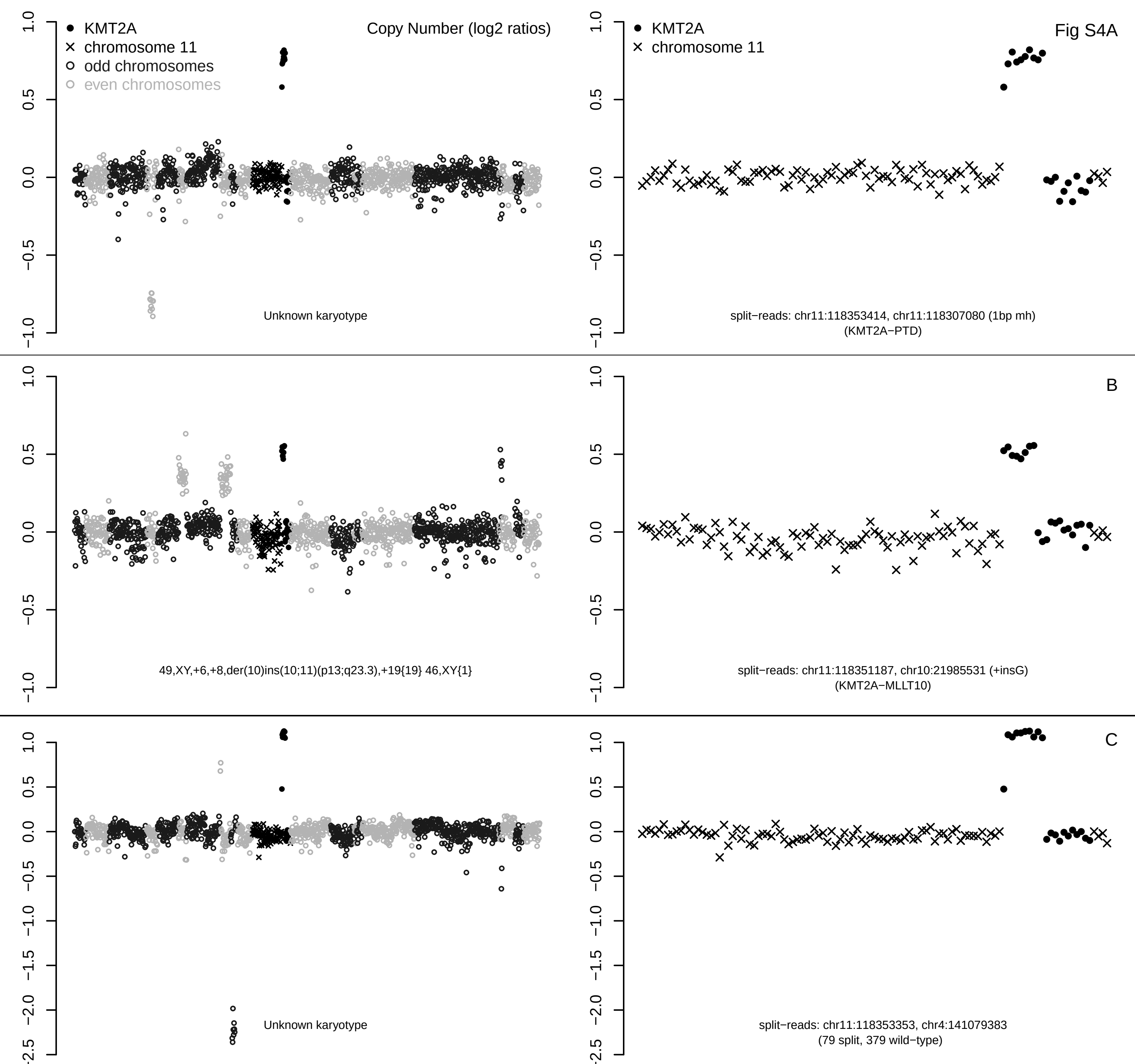
Fig S4A
Copy Number (log2 ratios)
● KMT2A
× chromosome 11
○ odd chromosomes
○ even chromosomes
1.0
0.5
0.0
−0.5
−1.0
Unknown karyotype
● KMT2A
× chromosome 11
split−reads: chr11:118353414, chr11:118307080 (1bp mh)
(KMT2A−PTD)
B
49,XY,+6,+8,der(10)ins(10;11)(p13;q23.3),+19{19} 46,XY{1}
split−reads: chr11:118351187, chr10:21985531 (+insG)
(KMT2A−MLLT10)
C
−1.5
−2.0
−2.5
Unknown karyotype
split−reads: chr11:118353353, chr4:141079383
(79 split, 379 wild−type)

Fig S5

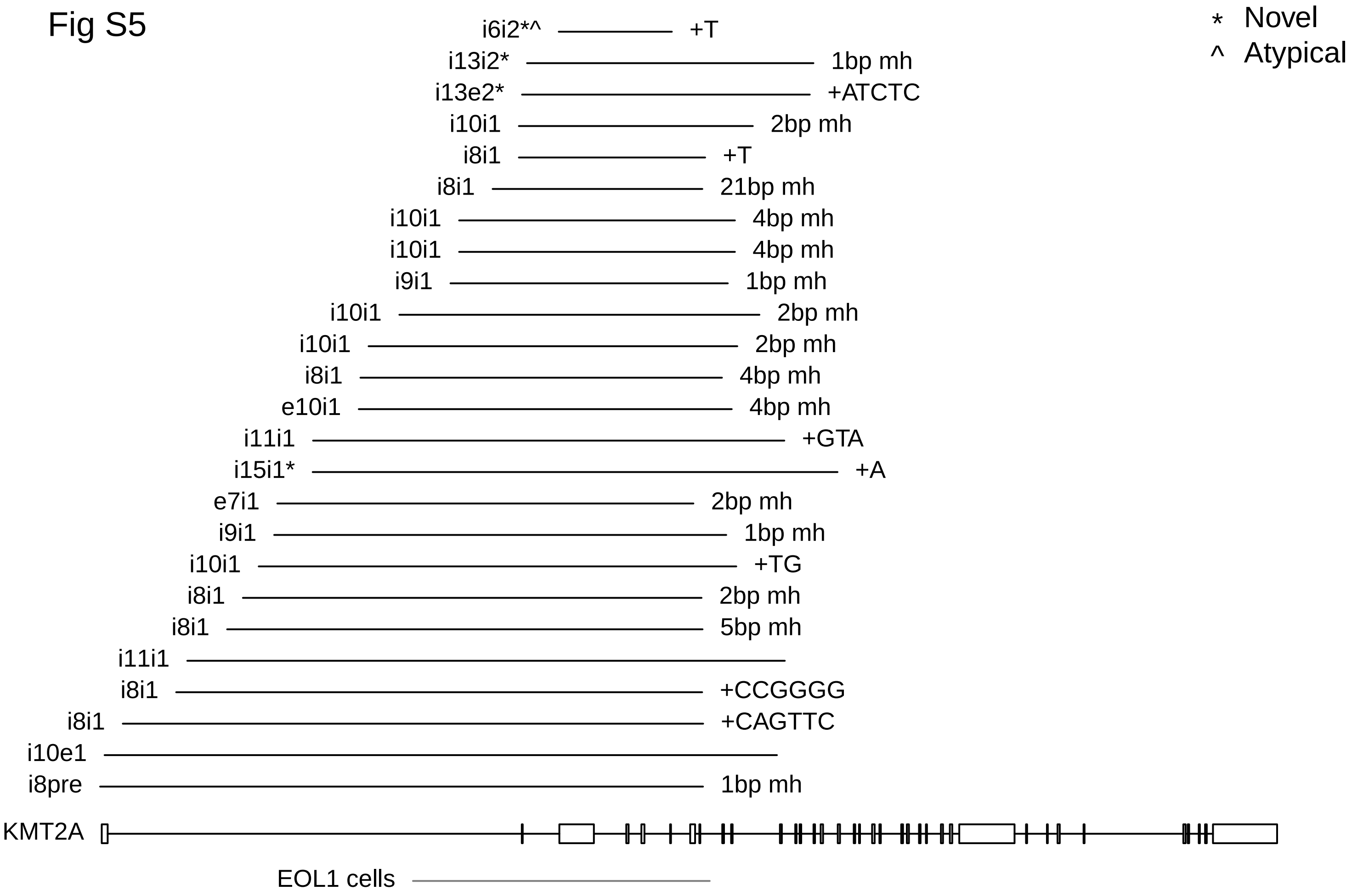
* Novel
^ Atypical
i6i2*^ +T
i13i2* 1bp mh
i13e2* +ATCTC
i10i1 2bp mh
i8i1 +T
i8i1 21bp mh
i10i1 4bp mh
i10i1 4bp mh
i9i1 1bp mh
i10i1 2bp mh
i10i1 2bp mh
i8i1 4bp mh
e10i1 4bp mh
i11i1 +GTA
i15i1* +A
e7i1 2bp mh
i9i1 1bp mh
i10i1 +TG
i8i1 2bp mh
i8i1 5bp mh
i11i1
i8i1 +CCGGGG
i8i1 +CAGTTC
i10e1
i8pre 1bp mh
KMT2A
EOL1 cells

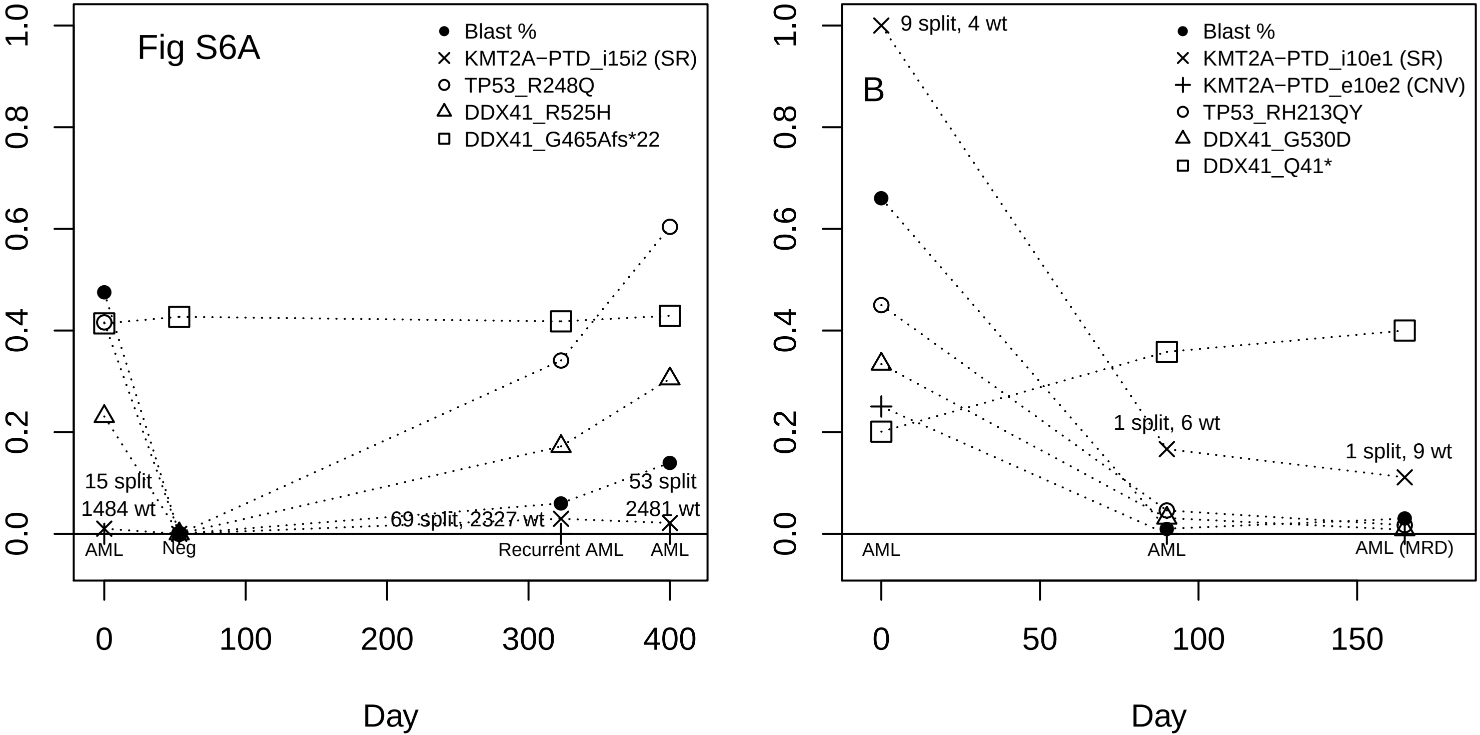
Fig S6A
Blast %
KMT2A−PTD_i15i2 (SR)
TP53_R248Q
DDX41_R525H
DDX41_G465Afs*22
15 split
1484 wt
69 split, 2327 wt
53 split
2481 wt
AML
Neg
Recurrent AML
AML
0.0
0.2
0.4
0.6
0.8
1.0
0
100
200
300
400
Day
B
Blast %
KMT2A−PTD_i10e1 (SR)
KMT2A−PTD_e10e2 (CNV)
TP53_RH213QY
DDX41_G530D
DDX41_Q41*
9 split, 4 wt
1 split, 6 wt
1 split, 9 wt
AML
AML
AML (MRD)
0.0
0.2
0.4
0.6
0.8
1.0
0
50
100
150
Day

KMT2A−PTD status at diagnosis

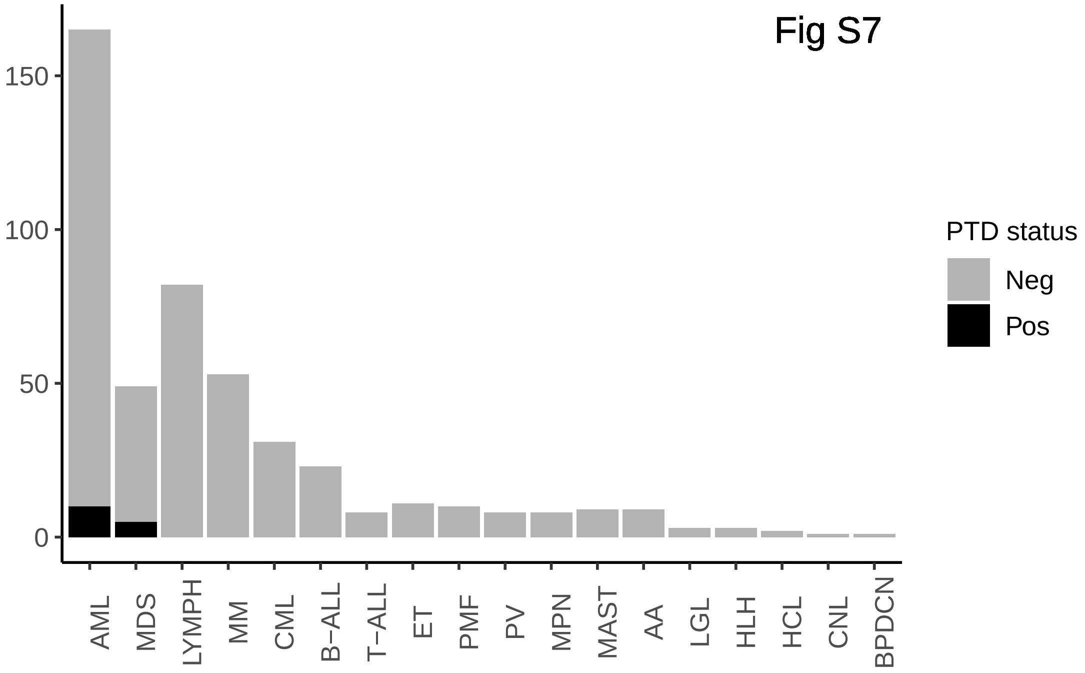

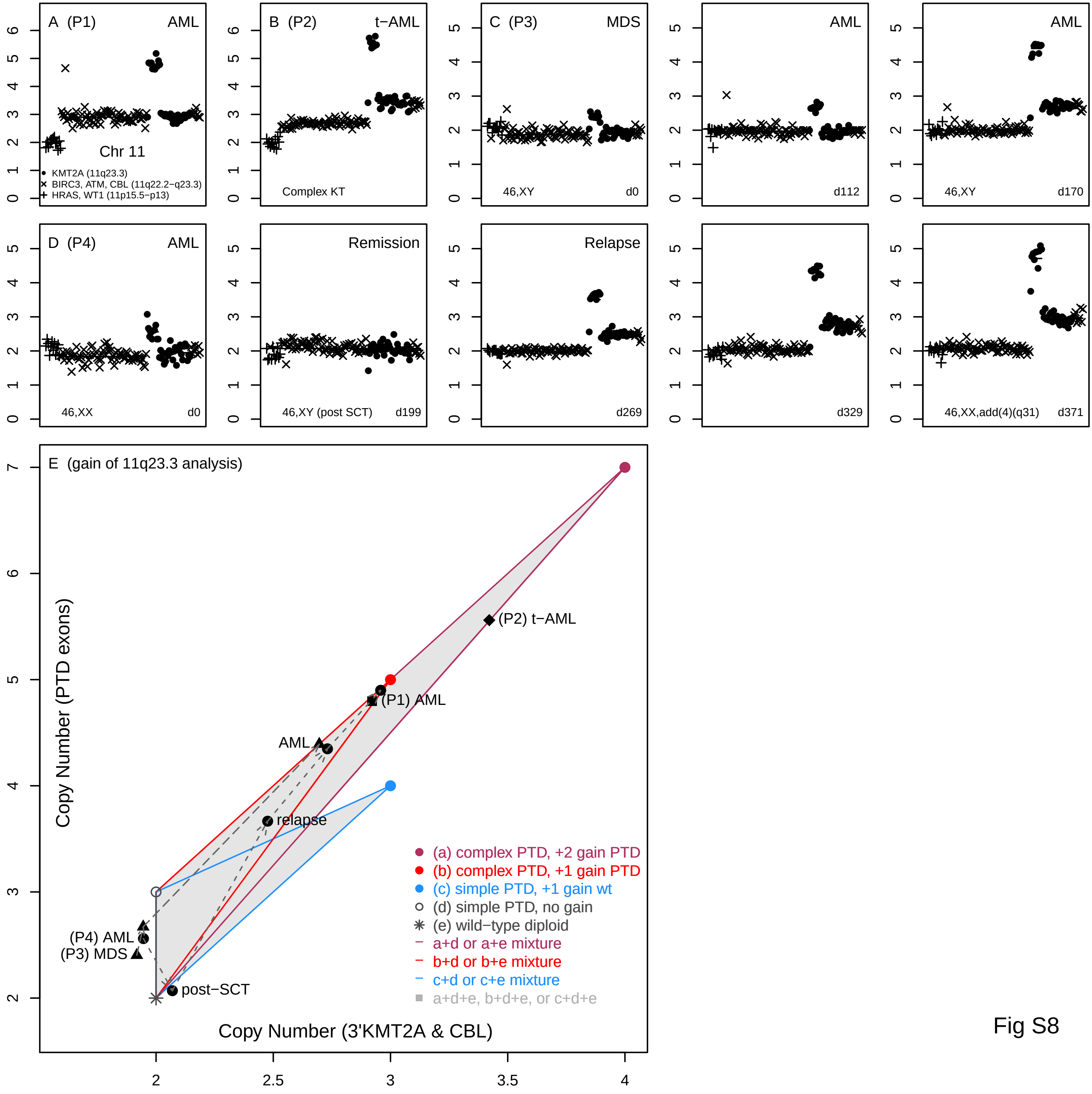
A (P1) AML
Chr 11
● KMT2A (11q23.3)
× BIRC3, ATM, CBL (11q22.2−q23.3)
+ HRAS, WT1 (11p15.5−p13)
B (P2) t−AML
Complex KT
C (P3) MDS
46,XY
d0
AML
d112
AML
46,XY
d170
D (P4) AML
46,XX
d0
Remission
46,XY (post SCT)
d199
Relapse
d269
d329
46,XX,add(4)(q31)
d371
0
1
2
3
4
5
6
E (gain of 11q23.3 analysis)
(P2) t−AML
(P1) AML
AML
relapse
(P4) AML
(P3) MDS
post−SCT
● (a) complex PTD, +2 gain PTD
● (b) complex PTD, +1 gain PTD
● (c) simple PTD, +1 gain wt
○ (d) simple PTD, no gain
✳ (e) wild−type diploid
− a+d or a+e mixture
− b+d or b+e mixture
− c+d or c+e mixture
■ a+d+e, b+d+e, or c+d+e
Copy Number (PTD exons)
Copy Number (3'KMT2A & CBL)
2
2.5
3
3.5
4
7

Fig S8

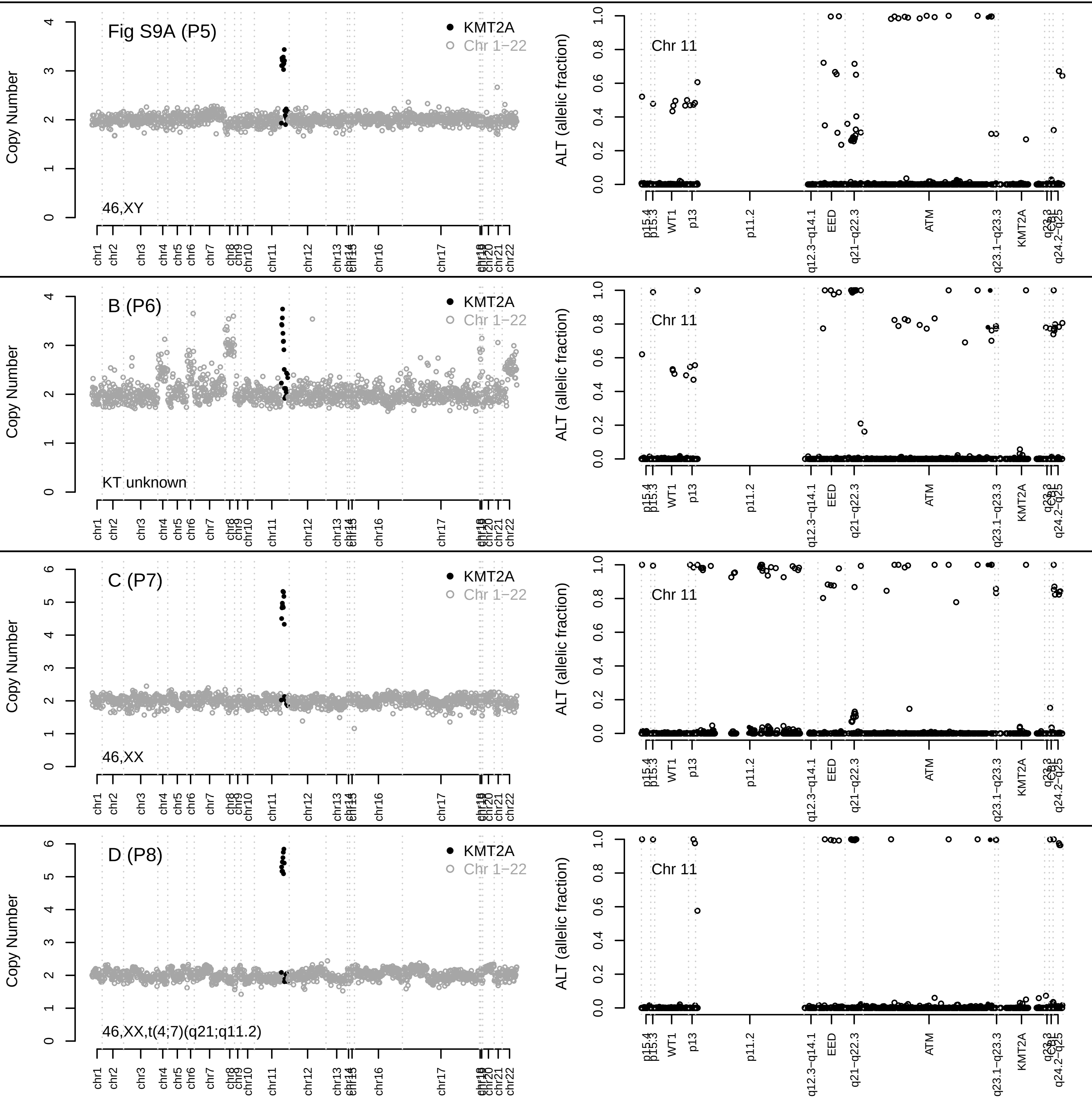
Fig S9A (P5)
KMT2A
Chr 1−22
Copy Number
0
1
2
3
4
46,XY
chr1
chr2
chr3
chr4
chr5
chr6
chr7
chr8
chr9
chr10
chr11
chr12
chr13
chr14
chr15
chr16
chr17
chr18
chr19
chr20
chr21
chr22
Chr 11
ALT (allelic fraction)
0.0
0.2
0.4
0.6
0.8
1.0
p15.4
p15.3
WT1
p13
p11.2
q12.3−q14.1
EED
q21−q22.3
ATM
q23.1−q23.3
KMT2A
q23.3
q24.1
q24.2−q25
B (P6)
KMT2A
Chr 1−22
Copy Number
KT unknown
Chr 11
ALT (allelic fraction)
C (P7)
KMT2A
Chr 1−22
Copy Number
0
1
2
3
4
5
6
46,XX
Chr 11
ALT (allelic fraction)
D (P8)
KMT2A
Chr 1−22
Copy Number
46,XX,t(4;7)(q21;q11.2)
Chr 11
ALT (allelic fraction)

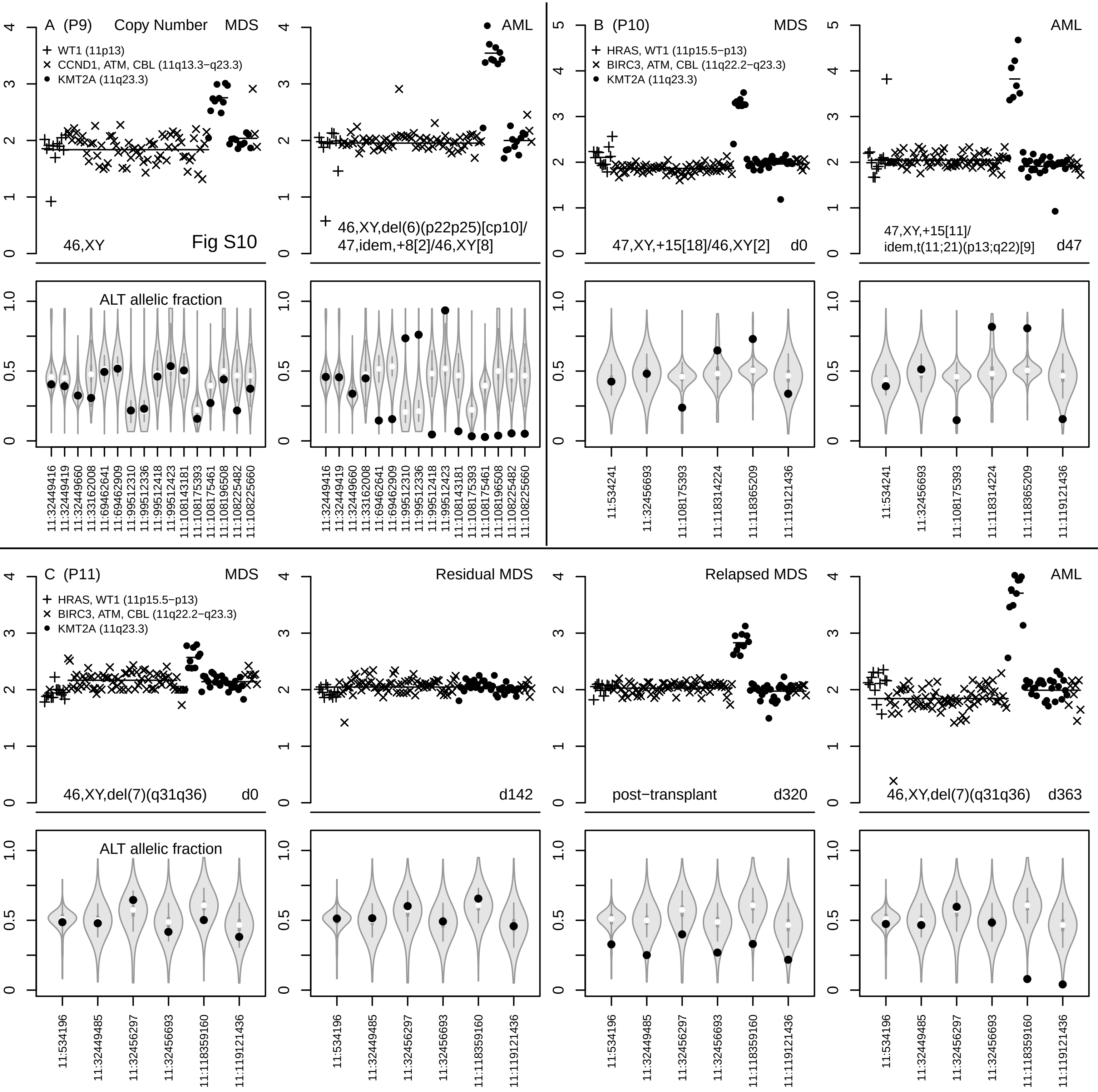
A (P9)
Copy Number
MDS
AML
+ WT1 (11p13)
× CCND1, ATM, CBL (11q13.3−q23.3)
● KMT2A (11q23.3)
46,XY
46,XY,del(6)(p22p25)[cp10]/
47,idem,+8[2]/46,XY[8]
ALT allelic fraction
11:32449416
11:32449419
11:32449660
11:33162008
11:69462641
11:69462909
11:99512310
11:99512336
11:99512418
11:99512423
11:108143181
11:108175393
11:108175461
11:108196508
11:108225482
11:108225660
B (P10)
MDS
AML
+ HRAS, WT1 (11p15.5−p13)
× BIRC3, ATM, CBL (11q22.2−q23.3)
● KMT2A (11q23.3)
47,XY,+15[18]/46,XY[2]
d0
47,XY,+15[11]/
idem,t(11;21)(p13;q22)[9]
d47
11:534241
11:32456693
11:108175393
11:118314224
11:118365209
11:119121436
C (P11)
MDS
Residual MDS
Relapsed MDS
AML
+ HRAS, WT1 (11p15.5−p13)
× BIRC3, ATM, CBL (11q22.2−q23.3)
● KMT2A (11q23.3)
46,XY,del(7)(q31q36)
d0
d142
post−transplant
d320
46,XY,del(7)(q31q36)
d363
ALT allelic fraction
11:534196
11:32449485
11:32456297
11:32456693
11:118359160
11:119121436
0
1
2
3
4
5
0
0.5
1.0

Fig S10

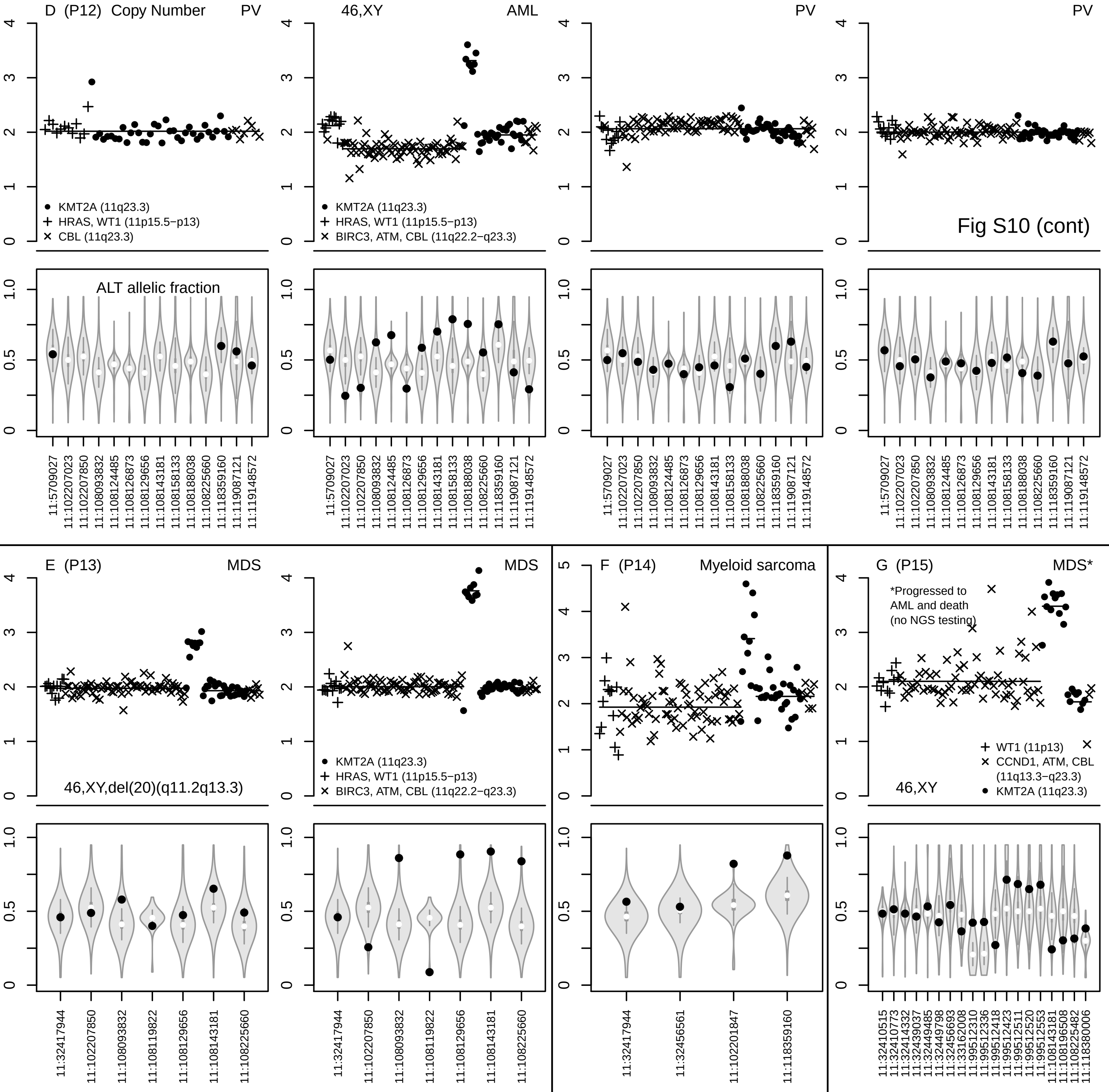

Fig S10 (cont)

D (P12) Copy Number
PV
46,XY
AML
PV
PV
● KMT2A (11q23.3)
+ HRAS, WT1 (11p15.5−p13)
× CBL (11q23.3)
● KMT2A (11q23.3)
+ HRAS, WT1 (11p15.5−p13)
× BIRC3, ATM, CBL (11q22.2−q23.3)
ALT allelic fraction
0
1
2
3
4
0
0.5
1.0
11:5709027
11:102207023
11:102207850
11:108093832
11:108124485
11:108126873
11:108129656
11:108143181
11:108158133
11:108188038
11:108225660
11:118359160
11:119087121
11:119148572
E (P13)
MDS
46,XY,del(20)(q11.2q13.3)
MDS
● KMT2A (11q23.3)
+ HRAS, WT1 (11p15.5−p13)
× BIRC3, ATM, CBL (11q22.2−q23.3)
11:32417944
11:102207850
11:108093832
11:108119822
11:108129656
11:108143181
11:108225660
F (P14)
Myeloid sarcoma
5
11:32417944
11:32456561
11:102201847
11:118359160
G (P15)
MDS*
*Progressed to AML and death (no NGS testing)
+ WT1 (11p13)
× CCND1, ATM, CBL (11q13.3−q23.3)
● KMT2A (11q23.3)
46,XY
11:32410515
11:32410773
11:32414332
11:32439037
11:32449485
11:32449798
11:32456693
11:33162008
11:99512310
11:99512336
11:99512418
11:99512423
11:99512511
11:99512520
11:99512553
11:108143181
11:108196508
11:108225482
11:118380006

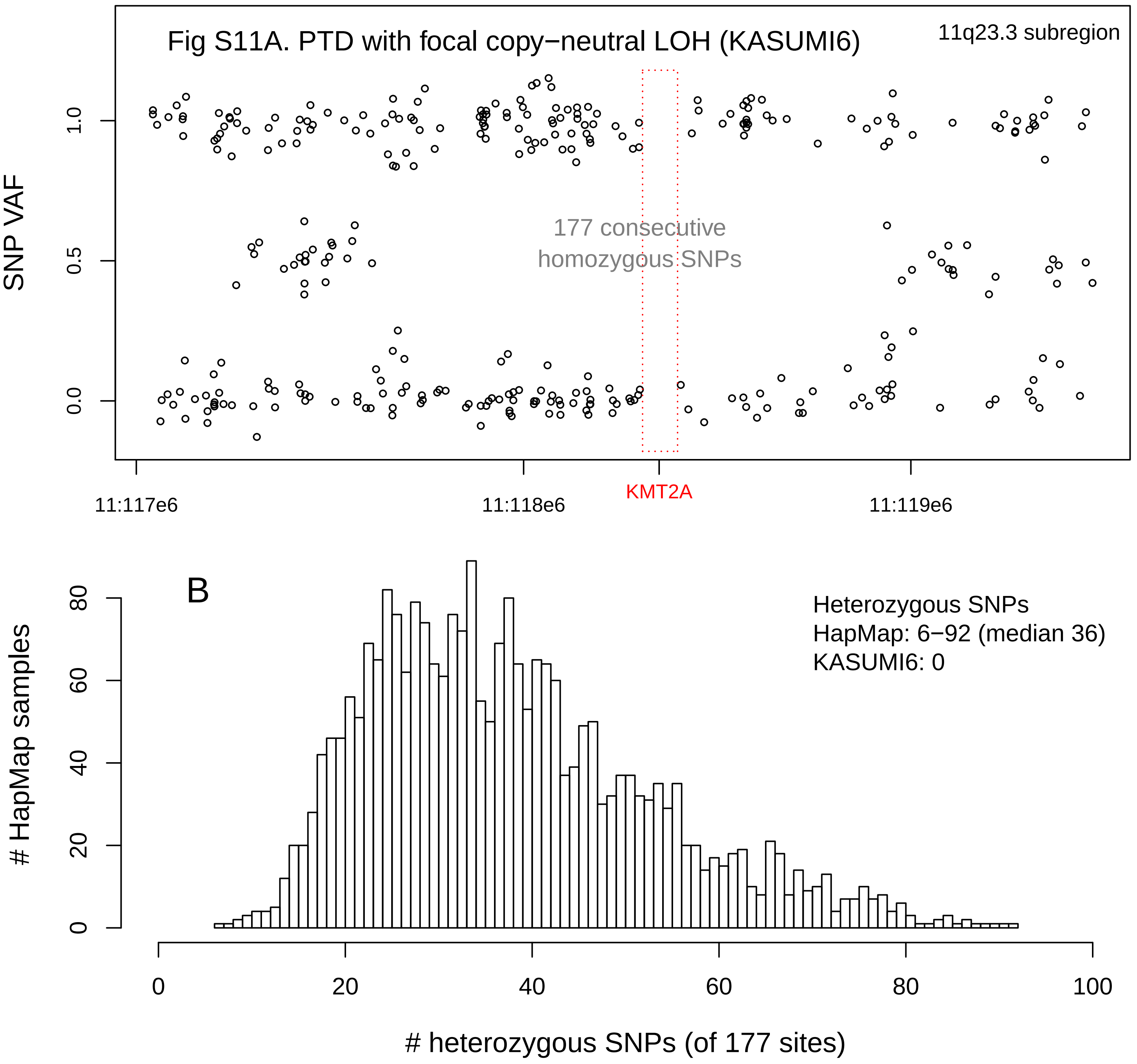
Fig S11A. PTD with focal copy−neutral LOH (KASUMI6)
11q23.3 subregion
SNP VAF
0.0
0.5
1.0
177 consecutive
homozygous SNPs
11:117e6
11:118e6
KMT2A
11:119e6
B
Heterozygous SNPs
HapMap: 6−92 (median 36)
KASUMI6: 0
# HapMap samples
0
20
40
60
80
0
20
40
60
80
100
# heterozygous SNPs (of 177 sites)

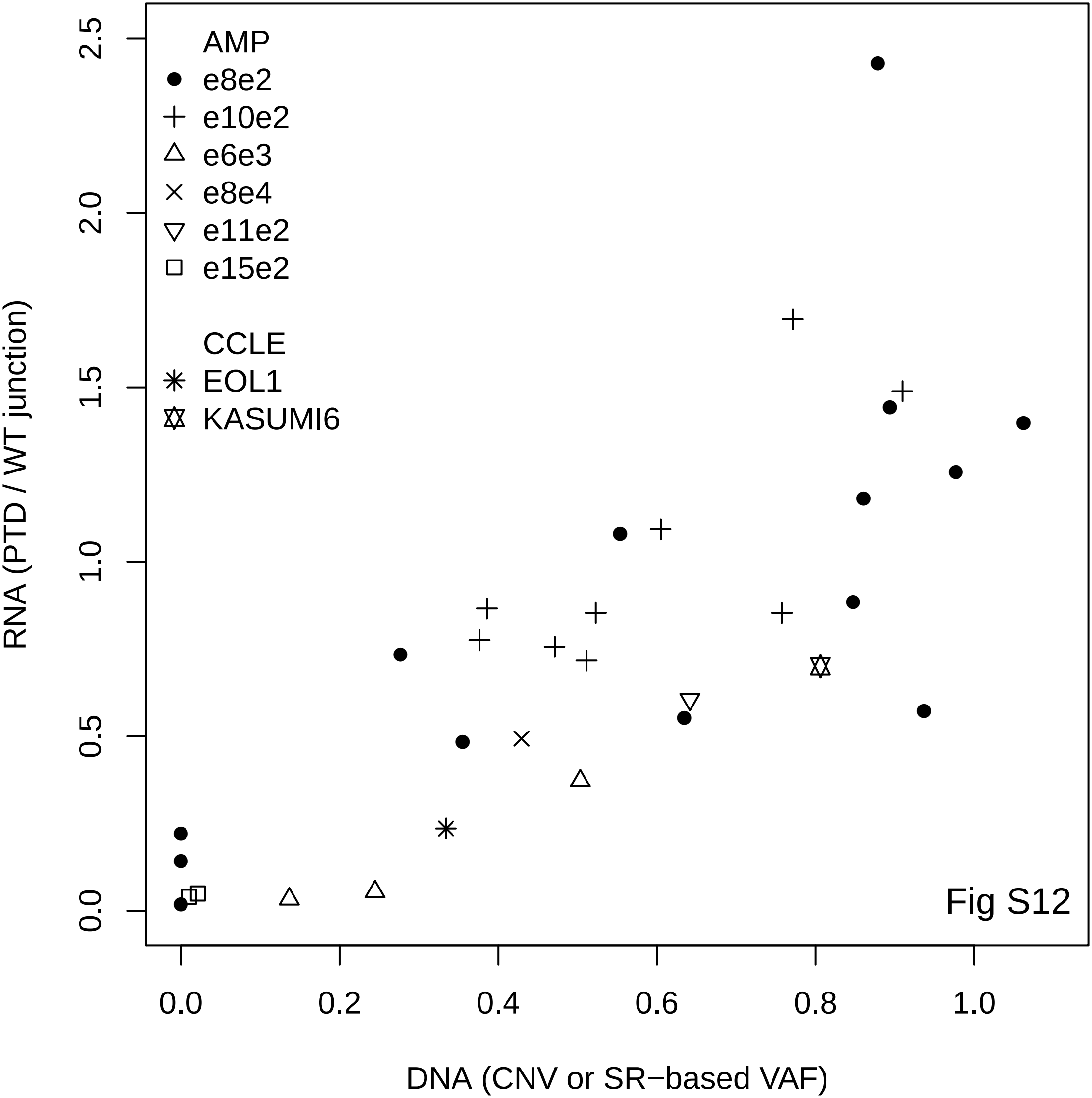
AMP
● e8e2
+ e10e2
△ e6e3
× e8e4
▽ e11e2
□ e15e2
CCLE
✳ EOL1
✡ KASUMI6
Fig S12
RNA (PTD / WT junction)
0.0
0.5
1.0
1.5
2.0
2.5
DNA (CNV or SR−based VAF)
0.0
0.2
0.4
0.6
0.8
1.0

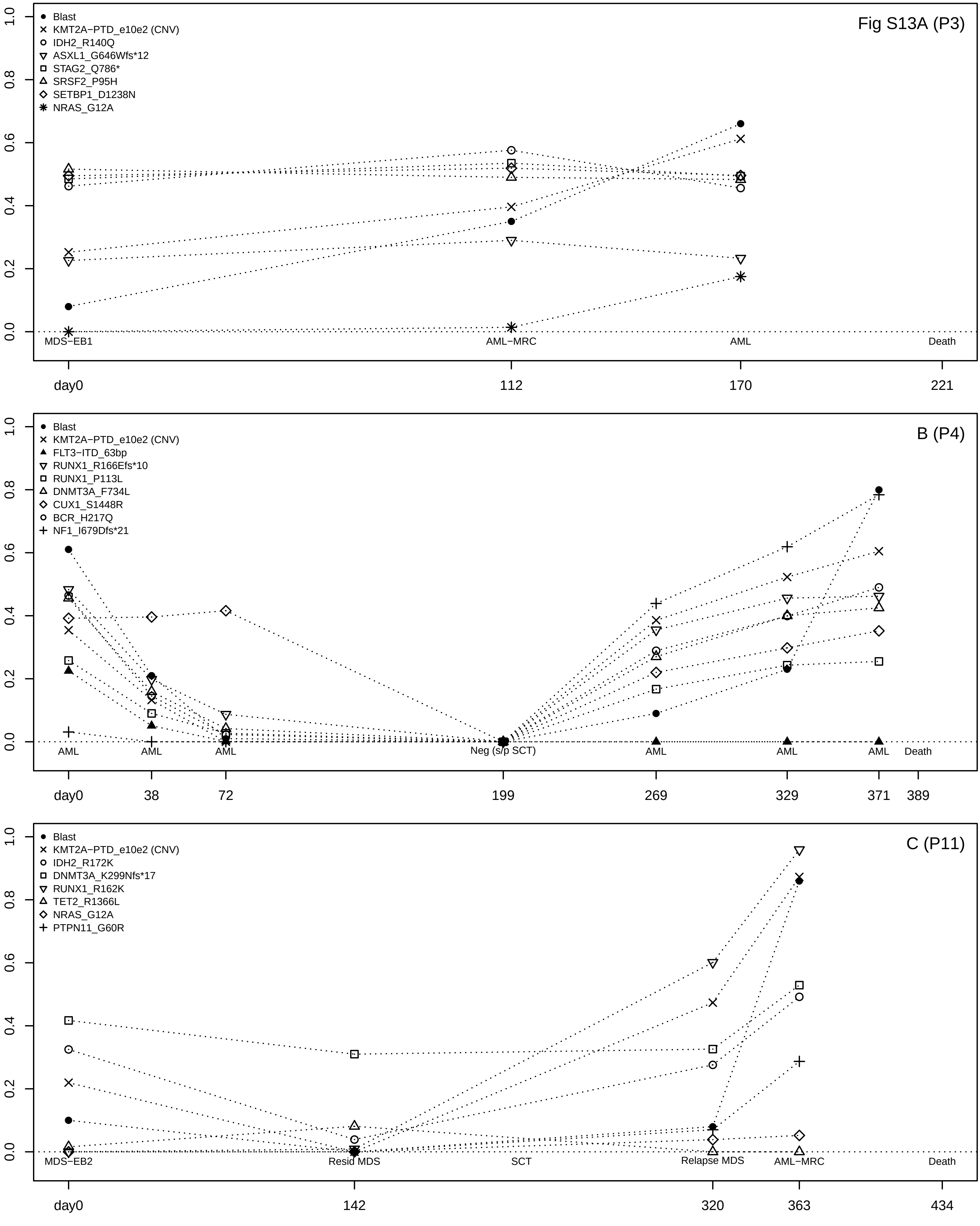

Fig S13A (P3)
● Blast
× KMT2A−PTD_e10e2 (CNV)
○ IDH2_R140Q
▽ ASXL1_G646Wfs*12
□ STAG2_Q786*
△ SRSF2_P95H
◇ SETBP1_D1238N
✳ NRAS_G12A
0.0
0.2
0.4
0.6
0.8
1.0
MDS−EB1
AML−MRC
AML
Death
day0
112
170
221
B (P4)
● Blast
× KMT2A−PTD_e10e2 (CNV)
▲ FLT3−ITD_63bp
▽ RUNX1_R166Efs*10
□ RUNX1_P113L
△ DNMT3A_F734L
◇ CUX1_S1448R
○ BCR_H217Q
+ NF1_I679Dfs*21
0.0
0.2
0.4
0.6
0.8
1.0
AML
AML
AML
Neg (s/p SCT)
AML
AML
AML
Death
day0
38
72
199
269
329
371
389
C (P11)
● Blast
× KMT2A−PTD_e10e2 (CNV)
○ IDH2_R172K
□ DNMT3A_K299Nfs*17
▽ RUNX1_R162K
△ TET2_R1366L
◇ NRAS_G12A
+ PTPN11_G60R
0.0
0.2
0.4
0.6
0.8
1.0
MDS−EB2
Resid MDS
SCT
Relapse MDS
AML−MRC
Death
day0
142
320
363
434

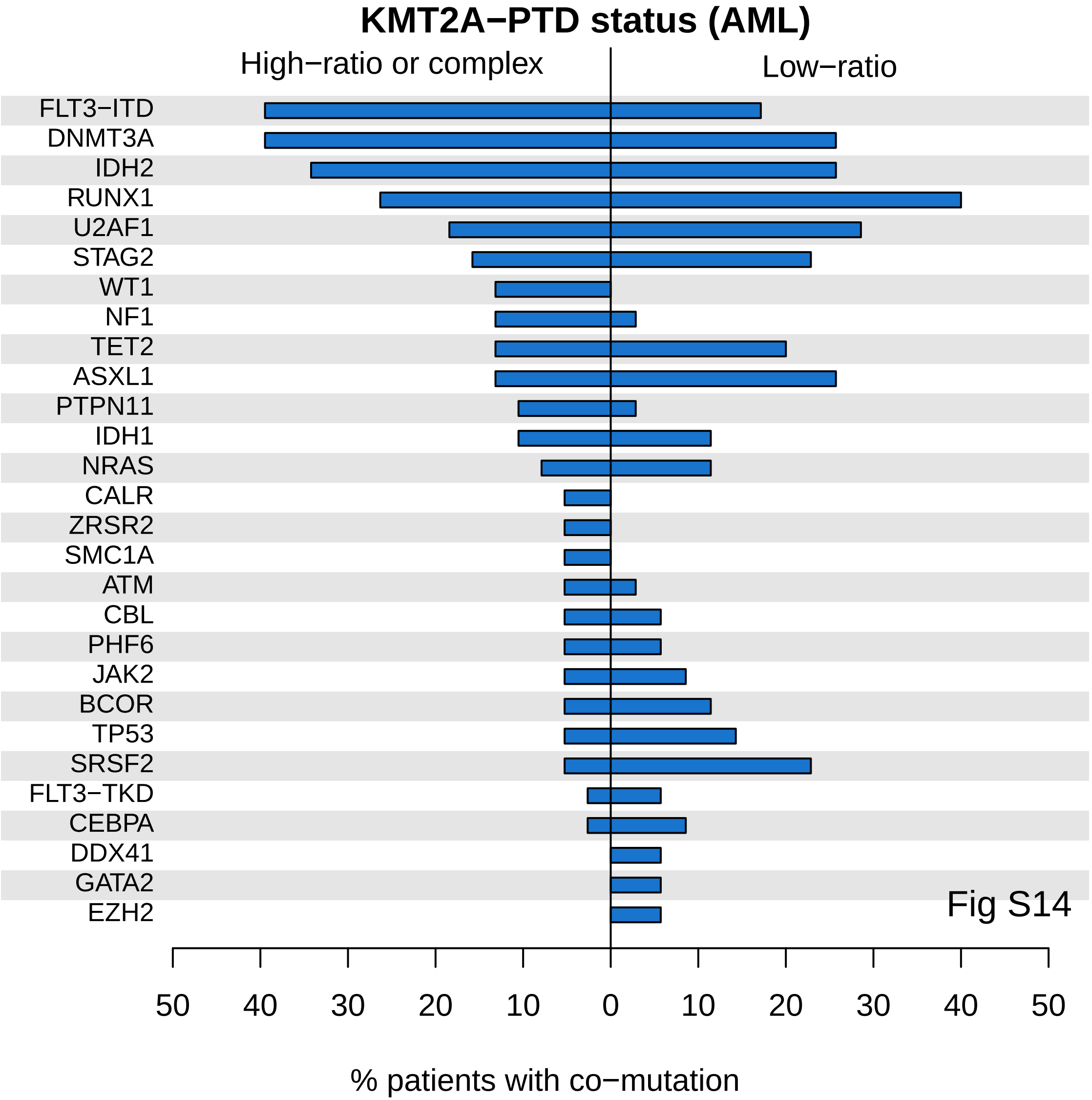
KMT2A−PTD status (AML)
High−ratio or complex
Low−ratio
FLT3−ITD
DNMT3A
IDH2
RUNX1
U2AF1
STAG2
WT1
NF1
TET2
ASXL1
PTPN11
IDH1
NRAS
CALR
ZRSR2
SMC1A
ATM
CBL
PHF6
JAK2
BCOR
TP53
SRSF2
FLT3−TKD
CEBPA
DDX41
GATA2
EZH2
50
40
30
20
10
0
10
20
30
40
50
% patients with co−mutation

Fig S14

Fig S15A

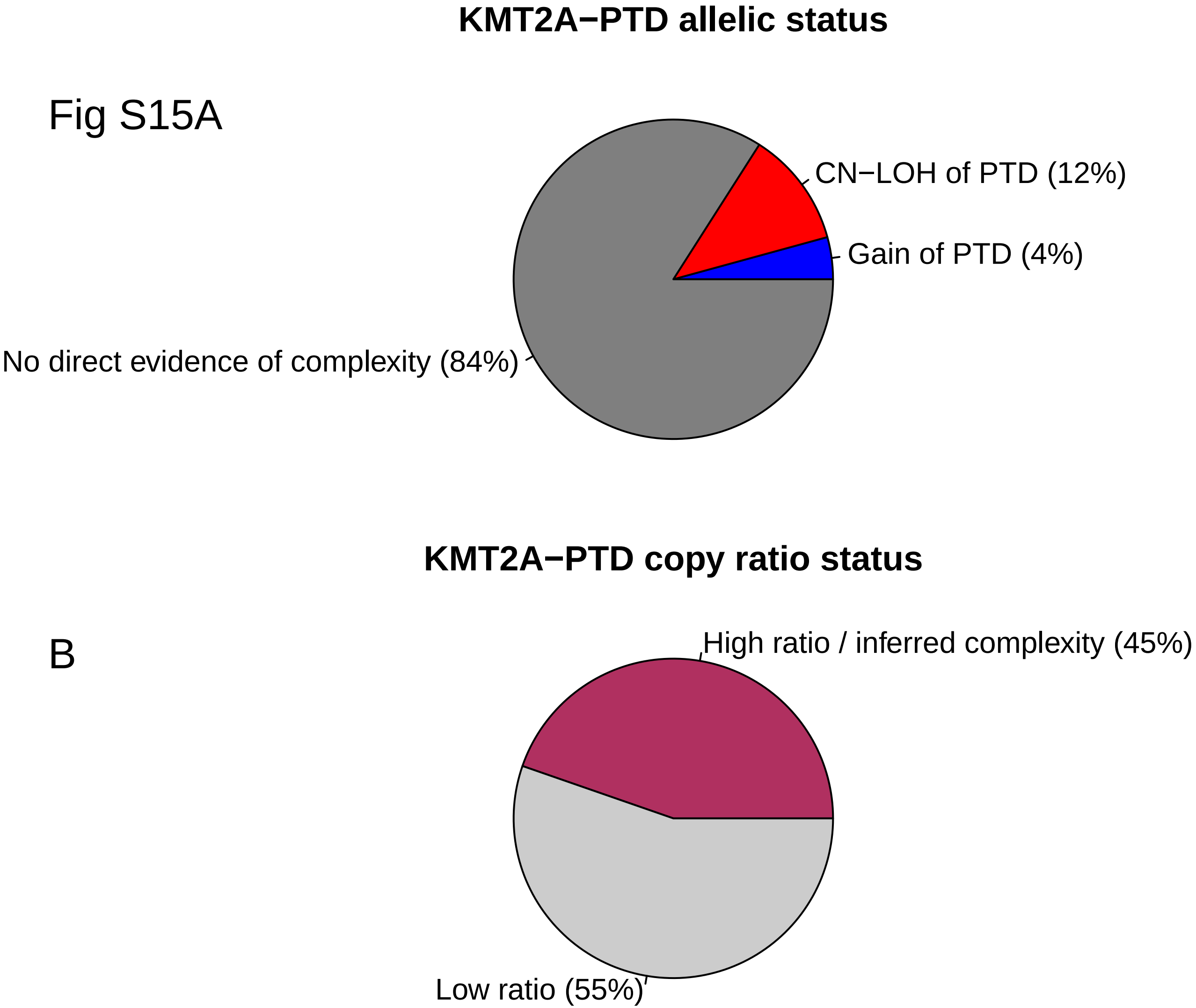

KMT2A−PTD allelic status
CN−LOH of PTD (12%)
Gain of PTD (4%)
No direct evidence of complexity (84%)
B
KMT2A−PTD copy ratio status
High ratio / inferred complexity (45%)
Low ratio (55%)